Journal of Coastal Research	00	0	000–000	Coconut Creek, Florida	Month 0000

Characterization of Bottom Sediments in the Río de la Plata Estuary

Diego Moreira[†‡]*, Claudia G. Simionato[†‡], Walter Dragani[‡§], Florence Cayocca[††], and Moira Luz Clara Tejedor[†‡]**

[†]Centro de Investigaciones del Mar y la Atmósfera (CIMA/CONICET-UBA)
Instituto Franco-Argentino para el Estudio del Clima y sus Impactos (UMI IFAECI/CNRS-CONICET-UBA)
Ciudad Autónoma de Buenos Aires C1428EGA, Argentina

[‡]Departamento de Ciencias de la Atmósfera y los Océanos, FCEN
Universidad de Buenos Aires
Ciudad Autónoma de Buenos Aires C1428EGA, Argentina

[§]Servicio de Hidrografía Naval Argentino (SHN)
Ciudad Autónoma de Buenos Aires C1270ABV, Argentina

[††]Institut Français de Recherche pour l'Exploitation de la Mer (IFREMER)
29280 Plouzane, Brest, France

www.cerf-jcr.org

www.JCRonline.org

ABSTRACT

Moreira, D.; Simionato, C.G.; Dragani, W.; Cayocca, F., and Luz Clara T., M., 0000. Characterization of bottom sediments in the Río de la Plata estuary. *Journal of Coastal Research,* 00(0), 000–000. Coconut Creek (Florida), ISSN 0749-0208.

Bottom sediments and surface water samples were collected in the intermediate and outer Río de la Plata (RDP) estuary, South America, during 2009–10, in six repeated cruises, with 26 stations each. Samples were processed for grain size and for water and organic matter content. The aim of this work is to analyze this new data set to provide a comprehensive and objective characterization of the bottom sediment distribution, to study the composition, and to construct a conceptual model of the involved physical mechanisms. Principal components analysis is applied to the bottom sediment size histograms to investigate the spatial patterns. Variations in grain size parameters contain information on possible sediment transport patterns, which were analyzed by means of trend vectors. Sediments show a gradational arrangement of textures: sand dominant at the head, silt in the intermediate estuary, and clayey silt and clay at its mouth. Textures become progressively more poorly sorted offshore, and the water and organic matter content increase and seem to be strongly related to the geometry and the hydrodynamics. Along the northern coast of the intermediate RDP, well-sorted medium and fine silt predominates, whereas along the southern coast, coarser and less sorted silt prevails from differences in tidal currents, in the tributaries' water pathways, or both. Around Barra del Indio, clay prevails over silt and sand, and the water and organic matter content reach a maximum, probably because of flocculation and reduction of the currents. Immediately seaward of the bottom salinity front, net transport reverses its direction, and well-sorted, coarser sand from the adjacent shelf dominates. Relict sediment is observed between the Santa Lucía River and Montevideo, consisting of poorly sorted fine silt and clay. The inferred net transport suggests convergence at the bottom salinity front, where the limit of the estuarine deposits is observed.

ADDITIONAL INDEX WORDS: *In situ observations, grain size distribution, grain size trend analysis, sedimentology, net sediment transport.*

INTRODUCTION

Between 15,000 and 20,000 million tons y^{-1} of suspended sediments reach the oceans in the entire world (Walling and Webb, 1996), 95% of them being carried by rivers (Syvitski, 2003). The amount of sediments transported by the Río de la Plata estuary, South America (Figure 1), has been estimated to more than 160 million tons y^{-1} (Menéndez and Sarubbi, 2007), representing more than 1% of the global estimation. Consequently, this estuary is one of the most turbid in the world, with extreme concentrations reaching more than 400 mg L^{-1} (Framiñan and Brown, 1996; Moreira *et al.*, 2013), and has an obvious effect on the adjacent shelf. It has been estimated that 90% (145 million tons y^{-1}) of the sediments that reach the Río de la Plata (RDP) as suspended sediments are silts and clays, whereas around 10 million tons y^{-1} correspond to very fine sands (Sarubbi, 2007). Coarse sands are transported as bed load and have been estimated to 15 million tons y^{-1} (Amsler, 1995; Amsler and Drago, 1988). Those sediments come mainly from the Paraná River, the main tributary to the RDP, which reaches the estuary after forming a large delta with two main branches: the Paraná Guazú to the north and the Paraná de las Palmas to the south (Figure 1). In contrast, the second main tributary, the Uruguay River, has a much smaller sediment load (Menéndez *et al.*, 2009). The drainage of a number of small tributaries along the Argentinean coast contributes to a minor part of the total solid discharge to the estuary.

Besides its geographical extension, the RDP is of large social, ecological, and economic importance for the countries along its

DOI: 10.2112/JCOASTRES-D-15-00078.1 received 7 May 2015; accepted in revision 19 October 2015; corrected proofs received XX Month XXXX; published pre-print online XX Month XXXX.
**Present address: Instituto Nacional de Investigación y Desarrollo Pesquero (INIDEP), B7602HSA, Mar del Plata, Pcia. de Bs.As., Argentina
*Corresponding author: moreira@cima.fcen.uba.ar

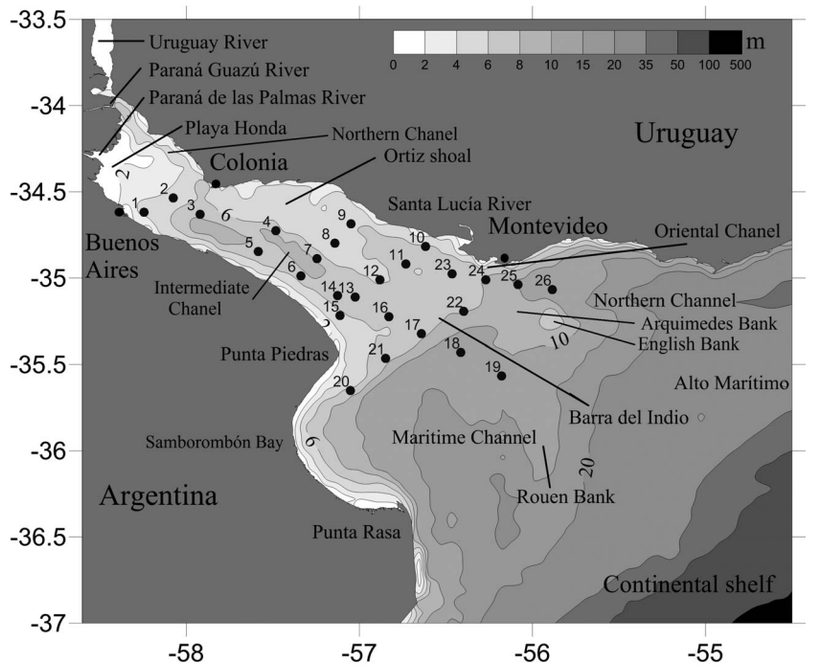

Figure 1. Study area, bathymetry, and geographical references. Black dots indicate the 26 sites where samples were collected during the six oceanographic cruises of the FREPLATA/FFEM experiment. The latitude and longitude of every sampling site is shown in Table 1.

shores, Argentina and Uruguay. The capital cities of both countries, Buenos Aires and Montevideo, and a number of harbors, resorts, and industrial centers are located on its margins and zone of influence. The estuary constitutes the main source of drinking water for the millions of inhabitants in the region, for whom it is also an important recreational area. The RDP is rich in nutrients and, therefore, has an abundant and diverse fauna. It shelters important fisheries and has the unusual feature of being both a spawning and nursery area for several coastal species (*e.g.*, Acha and Macchi, 2000; Berasategui, Acha, and Fernandez Araoz, 2004; Berasategui *et al.*, 2006; Rodrigues, 2005). Samborombón Bay is one of the most important wetlands of Argentina and is home to a number of species of fish, turtles, crabs, and migratory birds (Canevari *et al.*, 1998; Lasta, 1995). The freshwater plume of the RDP influences the shelf more than 500 km to the north (Campos *et al.*, 1999), exporting sediments, carbon, and nutrients.

In addition to land-ocean exchanges, many environmental questions in the RDP and the adjacent shelf are linked to the bottom sediment distribution and dynamics. The most significant issues include optimization of dredging operations (*e.g.*, Cardini, Garea, and Campos, 2002), understanding geomorphological change (*e.g.*, Codignotto *et al.*, 2012), contamination (*e.g.*, Colombo *et al.*, 2005, 2007), benthic ecology (*e.g.*, Gómez-Erache, 1999), primary productivity (*e.g.*, Gómez-Erache *et al.*, 2004; Huret *et al.*, 2005), and fisheries (*e.g.*, Jaureguizar *et al.*, 2003a,b; Jaureguizar, Militelli, and Guerrero, 2008). Nevertheless, the subject has received relatively little attention from the scientific community, especially during the last few decades. The distribution of surficial bottom sediments in the RDP was discussed by López Laborde (1987a,b), Parker *et al.* (1986a,b, 1987), Parker and López Laborde (1989), and Urien (1966, 1967, 1972), based on data from a number of diverse sources collected mostly during the 1960s and 1970s, and analyzed only the percentages of silt, clay, and sand present in the samples. More recently, López Laborde and Nagy (1999) compiled the results of the above-mentioned works and presented a re-elaborated map of the sediment distribution according to the Shepard (1954) diagram. Probably because of the nature of the available data, their figure is noisy and presents several features that are difficult to interpret in light of the most recent understanding of estuary hydrodynamics (*e.g.*, Framiñan *et al.*, 2008; Meccia *et al.*, 2009; Meccia, Simionato, and Guerrero 2013; Sepúlveda, Valle-Levinson, and Framiñan, 2004; Simionato *et al.*, 2004, 2006a, 2007). Moreover, distributions of water and organic matter content, histograms of the granulometric distribution, and simultaneous samples of suspended and bottom sediments were not available, which limited interpretation of the underlying physical processes.

The Environmental Protection of the Río de la Plata and its Maritime Front/French Fund for the Global Environment (FREPLATA/FFEM) experiment was performed between November 2009 and December 2010. It consisted of building a data base of new *in situ* observations that would overcome the limitations of the previous data bases, to help better understand the hydro-sedimentological processes in the estuary (Fossati, Cayocca, and Piedra-Cueva, 2014; Simionato *et al.,*

2011a,b) and to validate sediment dynamic numerical models. The experiment included six cruises with 26 oceanographic stations, during which, among other measurements, water and bottom sediment samples were collected in the intermediate and outer RDP. Particle size distributions (inferred from laser diffraction), as well as water and organic matter content, were derived for all samples, providing, for the first time, repeated and simultaneous measurements of those variables.

Moreira *et al*. (2013) presented a complete analysis of the suspended sediment samples collected during this experiment together with remotely sensed observations and time series of several physical variables. The purpose of this second paper is to analyze the data derived from the bottom sediment samples of this new data set, with the aim of providing a comprehensive and objective characterization of the long-term mean distribution of bottom surficial sediments in the RDP to study their composition, including the organic matter and water contents; to obtain a qualitative description of the mean transports; and to progress further in the construction of a conceptual model of the involved physical mechanisms. This knowledge is essential as a first step in the construction and validation of numerical models, which are needed for the estimation of the land-ocean fluxes and many other scientific and management purposes in this socially, economically, and ecologically important region.

This paper is organized as follows. Section 2 provides a description of the most relevant features of the study area. Section 3 describes sample acquisition and laboratory analysis. Section 4 discusses the methods applied to analyze the data. Section 5 presents the results of diverse analyses. Finally, Section 6 summarizes and discusses the results, building a conceptual model of the dominant sedimentological processes that occur in the different parts of the estuary and comparing the results of this study to those of previous studies.

Study Area

The RDP (Figure 1), located on the eastern coast of southern South America at approximately 35°S, is one of the largest estuaries in the world (Shiklomanov, 1998). It has a northwest to southeast–oriented funnel shape approximately 300 km long that narrows from 220 km at its mouth to 40 km at its upper end (Balay, 1961). The estuarine area is 35,000 km^2, and the fluvial drainage area is 3.1×10^6 km^2 (Framiñan *et al*., 1999).

The RDP displays a complex geometry and bathymetry. A complete description of its morphology can be found in Depetris and Griffin (1968), López Laborde (1987a,b), Ottman and Urien (1965, 1966), Parker *et al*. (1986a,b, 1987), and Urien (1966, 1967, 1972). The estuary is divided into two regions by the Barra del Indio shoal, a shallow area that crosses the estuary between Punta Piedras and Montevideo (Figure 1). The upper region is mainly occupied by fresh waters. Seaward of this shoal is the Maritime Channel, a wide depression 12–14 m deep in the north and 20 m deep in the south. It separates Samborombón Bay to the west from a region of banks known as Alto Marítimo (with depths ranging from 6 to 8 m) and the Rouen Bank (with depths between 10 and 12 m). The Oriental Channel, the deepest zone of the estuary with depths of up to 25 m, extends along the Uruguayan coast. Samborombón Bay is a very shallow and extensive area with depths ranging from 2 to 10 m extending south of Punta Piedras and up to Punta Rasa.

The RDP drains the waters of the Paraná and Uruguay rivers, which constitute the second largest basin of South America. It exhibits a very high discharge of around 22,000 m^3 s^{-1} on average and a peak discharge as high as almost 90,000 m^3 s^{-1} and as low as around 8,000 m^3 s^{-1} during extreme conditions related to the El Niño–Southern Oscillation cycles (Jaime and Menéndez, 2002). Density in the estuary is controlled by salinity, whereas temperature exhibits small horizontal gradients, even though interannual variability may be high (Guerrero *et al*., 1997; Simionato *et al.,* 2010). Water stratification is controlled by the confluence of highly buoyant continental discharge advecting offshore, lying on denser shelf waters that intrude into the estuary as a topographically controlled salt wedge. This salt wedge is typically between 100 and 250 km long (Guerrero *et al*., 1997) and defines a bottom salinity front over the Barra del Indio shoal following approximately the 10-m isobath (Guerrero *et al*., 1997). Forced by the prevailing winds (Simionato, Nuñez, and Engel, 2001), both surface and bottom salinity fronts show a seasonal cycle that largely modifies the salt wedge structure from spring–summer to fall–winter (Guerrero *et al*., 1997). The high wind variability that characterizes the region (Simionato, Vera, and Siegismund, 2005) also forces significant variability in synoptic time scales in the estuarine variables (Meccia *et al*., 2009; Meccia, Simionato, and Guerrero, 2013; Simionato *et al*., 2006a,b, 2007). Over long-term time scales, a spatial overlap has been observed between the bottom salinity front and an estuarine turbidity maximum characterized by elevated turbidity and high suspended sediment concentrations (Framiñan and Brown, 1996; Moreira *et al*., 2013).

The estuary is a microtidal system. Tidal waves associated with the South Atlantic amphidromes reach the Continental Shelf while propagating northward (O'Connor, 1991; Glorioso and Flather, 1995, 1997; Simionato *et al*., 2004). As they propagate over the shelf, the geographic setting modifies their propagation so that they enter the estuary mainly from the southeast (Simionato et al. 2004). The tide propagates at the phase speed (c) of the long external gravity waves $c = \lambda/T = \sqrt{gH}$, where λ is the wavelength, T is the period, g is the acceleration of gravity, and H is depth. In consequence, as the wave progresses toward the estuary mouth, H decreases; therefore, c and λ must decrease. Owing to this effect and the considerable length of the estuary, semidiurnal constituents have the unusual feature of a nearly complete wavelength within the estuary at all times (CARP 1989). Tidal amplitudes are not amplified toward the upper part. The estuary is long and converges only at its innermost part, where it is extremely shallow and bottom friction plays a fundamental role in controlling the wave amplitude (Framiñan *et al*., 2008; Simionato *et al*. 2004). As a result, tidal amplitudes and currents are larger along the southern coast of the estuary than along the northern coast. Maximum tidal current speeds occur along the southern coast of the estuary and, particularly, at the northernmost and southernmost limits of Samborombón Bay (Simionato *et al*., 2004).

Subtidal transport in the RDP is highly influenced by its geometry and bathymetry, the rotation of the Earth, and, especially, the winds (Simionato *et al*., 2004). In the upper estuary, after discharge, the flow concentrates along the deep

Table 1. *Number, geographical location (latitude and longitude), and depth of the* in situ *sampling sites shown as blue dots in Figure 1.*

Site	Latitude (S)	Longitude (W)	Depth (m)
1	34°37′	58°14′	3.7
2	34°30′	58°07′	3.7
3	34°37′	57°55′	5.7
4	34°43′	57°28′	5.4
5	34°50′	57°35′	6.2
6	34°59′	57°20′	6.2
7	34°53′	57°14′	6.2
8	34°37′	57°08′	5.1
9	34°41′	57°03′	5.4
10	34°49′	56°37′	7
11	34°55′	56°43′	5.7
12	35°00′	56°52′	5.3
13	35°06′	57°01′	4.8
14	35°06′	57°07′	5.2
15	35°12′	57°06′	5.2
16	35°13′	56°49′	5.2
17	35°19′	56°38′	6.2
18	35°25′	56°24′	11
19	35°33′	56°10′	10
20	35°39′	57°03′	4
21	35°27′	56°50′	5.5
22	35°12′	56°24′	6.8
23	34°58′	56°27′	6.1
24	35°00′	56°17′	7.5
25	35°02′	56°41′	9
26	35°03′	55°53′	12

north and intermediate channels. As the freshwater plume reaches the central part of the estuary, the rotation of the Earth (Coriolis effect) begins to be felt, and the transport concentrates to the north. Even though the Arquímedes and English banks divide the flow into two branches in the exterior part of the estuary, in the absence of winds, they meet again after flowing through this region. The transport increases (reduces) for higher (lower) runoff conditions, but the described pattern is preserved.

Simionato *et al*. (2004) divided the RDP into three regions with diverse responses to geometry, bathymetry, Earth's rotation, and winds. The upper part of the estuary has essentially a fluvial regime, mostly dominated by continental runoff and bathymetry. Its circulation pattern exhibits the smallest sensitivity to changes in winds. The second region is Samborombón Bay, dynamically isolated from the northern portion of the estuary. In the absence of wind, its circulation is weak and from the south, because of tidal rectification. This part of the estuary is very sensitive to wind direction. Finally, the exterior part of the estuary has more oceanic characteristics, and its circulation is not only related to discharge and bathymetry but also to the Earth's rotation and the thermohaline structure. The area is naturally sensitive to the winds.

The path of the different plumes of the main tributaries to the RDP along the upper and intermediate estuary have been studied by means of numerical simulations by Simionato, Meccia, and Dragani (2009). The waters of the major tributaries flow through the estuary forming three main plumes. The Uruguay and Paraná Guazú-Bravo waters mainly occupy the northern (Uruguayan) coast and the central part of the channel, with some mixing between them, whereas the Paraná de las Palmas waters flow along the southern (Argentinean) coast. The occurrence and pattern of the plumes are controlled by the runoff and geometry and bathymetry of the estuary. This way, the Uruguayan coast is mostly affected by waters of the Uruguay River and the Argentinean coast by waters of the Paraná de las Palmas.

In regard to the processes that drive the bottom sediment distribution in the RDP, Parker *et al*. (1987) interpreted the grain size observations available at that time and synthesized the various geological and oceanographic arguments to develop a first hypothesis for the processes associated with sediment transport and dispersion in the estuary. According to those authors, the upper RDP estuary would be divided into two parts, one to the north and other to the south—the northern one influenced by the Uruguay and the Paraná Guazú rivers and the southern one influenced by the Paraná de las Palmas and Luján (a tributary to Paraná) rivers. Upstream of the Santa Lucía River mouth and along the Uruguayan coast of the estuary, they suggest the presence of relict mud, whereas over the Barra del Indio shoal region, they suggest flocculation of clays. Finally, they identify the sands found in the exterior RDP as relict sediments.

METHODS

This section presents a different data set and the applied methodologies. The bottom sediment samples analyzed in this paper were collected between 2009 and 2010, during the FREPLATA/FFEM experiment funded by FFEM. Six oceanographic synoptic cruises approximately every 2 months were made during the experiment: in November 2009 and in March, June, August, October, and December 2010. Cruises lasted 2–3 days and visited the 26 sites listed in Table 1 and shown as black dots in Figure 1.

Data

This work analyzes the grain size distribution and water and organic matter content derived from the above-mentioned bottom sediment samples. Water and bottom sediment samples were collected by a Fly pump and a stainless steel Van Veen grab sampler, respectively. Water from the subsurface at a depth of approximately 2 m was collected in 20-L bottles, whereas bottom sediment samples were saved in sealed bags.

The grab sampler permitted the extraction of samples of roughly 0.1 m^3, belonging to the upper 20 cm of the bottom sediment layer. Only a small part of these samples, corresponding to their central part, was saved at each site for further analysis to avoid errors in the estimations from possible water leaks during the fast (because of the shallowness of the estuary) hoisting of the sampler.

Samples were analyzed at the Marine Geology Laboratory of the Hydrographic Service of the Navy of Argentina for water and organic matter content. Sediments destined for water content analysis were weighed, dried at 80°C for 1 week, cooled to room temperature, and finally weighed. Percent water was calculated as the difference between the weight before and after drying divided by the initial sample weight. To determine the organic matter content, samples were dried at 60°C for 1 week and then triturated. They were then weighed and transferred to a small pot for ignition at 450°C for 3 hours. The burnt sediments were transferred to a drying bell (with

silica gel) for 30 minutes to cool without absorbing external moisture and finally weighed. The organic matter content was estimated as the weight difference before and after ignition.

Grain size analyses were performed for the samples collected in cruises 2 to 6 in the Sedimentological Laboratory of the Geology Department of the University of Buenos Aires. A grain size analyzer using a laser diffraction optical system integrated with a charge-coupled device (CCD) camera (CILAS 1180) was used. This analysis allows the measurement of particles with diameters ranging from 0.04 to 2,500 μm. The smaller particles (0.04–500 μm) were measured capturing a diffraction pattern and applying the theory of Fraunhofer or Mie, whereas the coarser particles were measured using real-time Fourier transforms of the images captured by the CCD camera, which is equipped with a digital signal processing unit. Every sample was mechanically agitated for a few minutes to homogenize it. A representative portion of the sample was introduced into the analyzer, where the sediment was the object of ultrasonic vibration for 60 seconds before taking the measurement. The sediment was treated with a solution of 20% hydrogen peroxide (H_2O_2) for 2–3 weeks until complete removal of organic matter. Then, the samples were washed with distilled water and centrifuged at 20,000 rpm for 20 minutes to separate completely the solid and liquid fractions. The liquid fraction was discarded, and the solid fraction was transferred to glass jars (30 mL) and diluted with distilled water. When gravel size material was detected, usually from the presence of bivalve and gastropod shells, the sediment was sieved with sieve #10 so that only the fraction with diameters less than 2 mm was analyzed with the CILAS particle analyzer.

During the cruises, conductivity-temperature-depth and turbidity measurements were made at every station. These data were analyzed by Moreira *et al*. (2013). Their figure 6 shows maps of surface and bottom turbidity and salinity that can aid in the interpretation of the results discussed in this paper.

Statistical Methods

This study applied different statistical methods to the data described in the previous sections (Figure 1). To present the mean distributions (first and second panels of Figures 2 and 3) of the six repeated observations at each of the 26 sampled locations, the mean and standard deviation among samples were defined, respectively, as:

$$\bar{G} = \frac{1}{6}\Sigma_1^6 G_j \tag{1}$$

$$\sigma_G = \frac{1}{6}\left[\Sigma_1^6 (G_j - \bar{G})^2\right]^{\frac{1}{2}} \tag{2}$$

where G is the variable under analysis (percent sand, silt, clay, water, and organic matter content). This analysis has two aims: it not only allows study of the (long-term) means, but also permits the observation of the variability among samples, allowing the identification of the areas where the means are representative.

For every sample, the mean grain size, μ, standard deviation, σ, and skewness, S_k, were calculated using the statistic moment method (McManus, 1988):

$$\mu = \Sigma_1^n P_i S_i \tag{3}$$

$$\sigma = \left[\Sigma_1^n P_i (S_i - \mu)^2\right]^{\frac{1}{2}} \tag{4}$$

$$S_k = \left[\Sigma_1^n P_i (S_i - \mu)^3\right]^{\frac{1}{3}} \tag{5}$$

where i is size class, P_i is percentage of size S_i, and n is the total number of size classes.

Using the above-mentioned statistics, the degree of sorting, defined as the ratio between the standard deviation (Equation [4]) and mean grain size (Equation [3]) also were computed (Skene *et al*., 2005).

The sediments were classified according to Shepard (1954). The SEDPLOT tool (USGS CMGP, 2014) was used to construct the Shepard classification scheme in the Wentworth (1922) grade scale.

Principal components analysis (PCA; Preisendorfer, 1988) was applied to analyze the large number ($5 \times 26 = 130$) of different CILAS grain size histograms obtained from the five samples (cruises 2 to 6) collected at each of the 26 stations. A small signal-to-noise ratio might be responsible for a sediment distribution (particularly if the samples are multimodal) that has too much information in a few class intervals and too little in others. To avoid a possible effect on the results, the analysis was applied to the set of "anomalies," defined as the difference between a "mean histogram" (defined as the mean of all the available histograms) and each sample. After the analysis, the signal can be recomposed by simply adding the "mean histogram." The aim of PCA is to extract "characteristic histograms" objectively for different regions of the estuary and, therefore, reduce the dimensionality of the problem. This type of treatment allows taking into account the relationships (represented by the correlation matrix) among all the studied histograms. The PCA creates new characteristic histograms, the principal components (PCs), which are uncorrelated and are the eigenvectors of the correlation matrix. They are derived in decreasing order of importance so that, for example, the first PC accounts for as much as possible of the variance of the original data (the set of original histograms, in this case). The percentage of the total variance accounted for by each PC is interpreted as the portion "explained by" the characteristic histogram represented by the PC. In this case, this percentage will be directly proportional to the number of samples that are represented by the mode and, therefore, has no direct physical interpretation, except that a larger variance is probably related to a larger area. The most important point of PCA is that the PCs reveal groupings of histograms, outliers, or both that would be difficult to find by other means and that can be associated with sedimentological processes. The user has to look at the groups of characteristic histograms suggested by the PCs and consider whether the components have some meaningful interpretation or are simply mathematical artifacts. The PCA analysis discussed in this paper differs from the Shepard classification, also applied in this work, in that it takes into account not only the fractions of silt, clay, and sand, but also the shape of the grain size distribution (or histogram). Therefore, results can provide further information about

sedimentological processes. This analysis has been used by other authors with the same aim as in this work (*e.g.*, Cheng, Gaob, and Bokuniewicz, 2004; Skene *et al.*, 2005).

Possible sediment transport paths in the RDP were studied by applying grain size trend analysis. McLaren (1981) and McLaren and Bowles (1985) statistically related net sediment transport paths to spatial changes in the mean grain size (μ in Equation [3]), the variance (σ^2 in Equation [4]), and the skewness (S_k in Equation [5]) of the distribution. For two sampling sites d_1 and d_2, if the net transport direction is from d_1 to d_2, there are two cases of grain size changes from d_1 to d_2: case 1, $\sigma_2^2 \leq \sigma_1^2$ when $\mu_2 > \mu_1$ and $S_{k2} \leq S_{k1}$; case 2, $\sigma_2^2 \leq \sigma_1^2$ when $\mu_2 < \mu_1$ and $S_{k2} \geq S_{k1}$.

Gao and Collins (1991, 1992) developed a two-dimensional statistical model that derives an estimation of the net sediment transport patterns from the bottom sediment spatial distribution. The methods may be split into three consecutive steps. The first step consists of defining trend vectors for a grid of sampling sites by comparing each sample with its neighbors. To identify a "neighboring" site, a characteristic distance (D_{CR}) representing the space-scale of sampling, is specified. If the distance between any two sites is smaller than this characteristic distance, they are considered neighboring sites, and their grain size parameters are compared. If either a case 1 or case 2 trend (described previously) is identified between the two sites, then a dimensionless "trend" vector is defined for the site with the higher variance. The direction of such a vector runs from the site with a higher variance to that with a lower variance. The length of the vector is assumed, for convenience, to be unity. Second, at each sampling site, there may be more than one unit-length vector. Therefore, for such a site, vectors are added to produce a single vector:

$$\vec{\mathrm{R}}(x,y) = \Sigma_1^n \vec{\mathrm{r}}(x,y)_i \tag{6}$$

where n is the number of trend vectors identified for the site, $\vec{\mathrm{r}}(x, y)$ is a trend vector, and $\vec{\mathrm{R}}(x, y)$ is the sum of the trend vectors. Both the real transport trends and some noise are included in $\vec{\mathrm{R}}(x, y)$, although the amount of the noise may have been reduced already by the adding process. The third step consists in removing the noise included in the vectors at each site. It is assumed that the various components of noise do not exhibit any ordered pattern, so the noise may be removed by averaging the vectors of a particular sampling site with the vectors from adjoining sites. Once again, an adjoining site is assessed on the basis of the characteristic distance (D_{CR}) defined previously. The averaging procedure is equivalent to the following mathematical transformation for the site at which $\vec{\mathrm{R}}(x, y)$ is defined:

$$\vec{\mathrm{R}}_{\mathrm{av}}(x,y) = \frac{1}{k+1}\left[\vec{\mathrm{R}}(x,y) + \Sigma_1^k \vec{\mathrm{R}}_j\right] \tag{7}$$

where $\vec{\mathrm{R}}_j$ is a trend vector obtained from Equation (6) at a neighboring site and k is the total number of such sites. The vectors $\vec{\mathrm{R}}_{\mathrm{av}}$ can be defined as transport vectors; they form a residual pattern, with little influence from noise. If the residual trends have an ordered pattern in the arrangement of the transport vectors, then they should represent statistically and conceptually possible net transport paths. Then, the length of the characteristic vector is defined by:

$$L = \Sigma_1^N |\vec{\mathrm{R}}_{\mathrm{AV}}(x,y)_i| \tag{8}$$

Finally, the particle size of the suspended sediment was used to estimate settling velocity and correlate this information with the hydrodynamic conditions in different locations of the estuary. A simple but common description of particle settling velocity, provided by Stokes law, assumes small particle Reynolds and impermeable, spherical particles according to the formula:

$$w_{\mathrm{s}} = \frac{(\rho_{\mathrm{p}} - \rho_{\mathrm{w}})gd^2}{18\mu} \tag{9}$$

where w_{s} is the settling velocity, d the particle diameter, g the gravitational acceleration, ρ_{p} the particle density, ρ_{w} the water density, and μ the dynamic viscosity. The water density was estimated using the temperatures and salinities measured during the FREPLATA/FFEM experiment, at the same time sediment samples were collected. Even though the definition of settling velocity used is quite simplistic, it is enough for the purposes of this work, in which the attempt is only to compare the behavior of the suspended particles from one site of the RDP to another.

RESULTS

The results of the analysis of the different data with the above-mentioned methodologies are presented in this section. First shown are the percentages of silt, clay, and sand in the bottom sediments as the percentages of water and organic matter present in the samples. The degree of sorting and the diameter of the sediments complement the analysis. Analysis of the spatial bottom sediment distribution according to both Shepard and PCA allows a comparison of the granulometry of those areas with similar bottom sediments to the granulometry of the sediments suspended in the water column. Finally, the net sediment transport pathways are explored.

Mean Distribution of Bottom Sediments and Water and Organic Matter Contents

The mean percentage and standard deviation between samples in the Wentworth scale classification of sand (grain sizes between 62.5 and 250 μm), silt (grain sizes between 3.9 and 62.5 μm), and clay (grain sizes <3.9 μm), computed according to Equations (1) and (2), are shown in the upper, central, and lower panels of Figure 2, respectively. Numerical values at every station are provided in Table 2.

The concentration of sand (Figure 2, upper left panel) is at its maximum in the outer estuary, where it connects to the adjacent Continental Shelf. There, percent sand reaches 70% and mean grain size is around 180 μm (Table 2), which is much coarser than for the other sampled sites. The standard deviation (Figure 2, upper right panel) is low (<5%), indicating low variability between samples. A low percentage (<10%) of very fine sands (with sizes <70 μm; Table 2) is observed in the upper estuary and along the southern (Argentinean) coast of the intermediate estuary, with a relatively higher standard deviation (up to 7%).

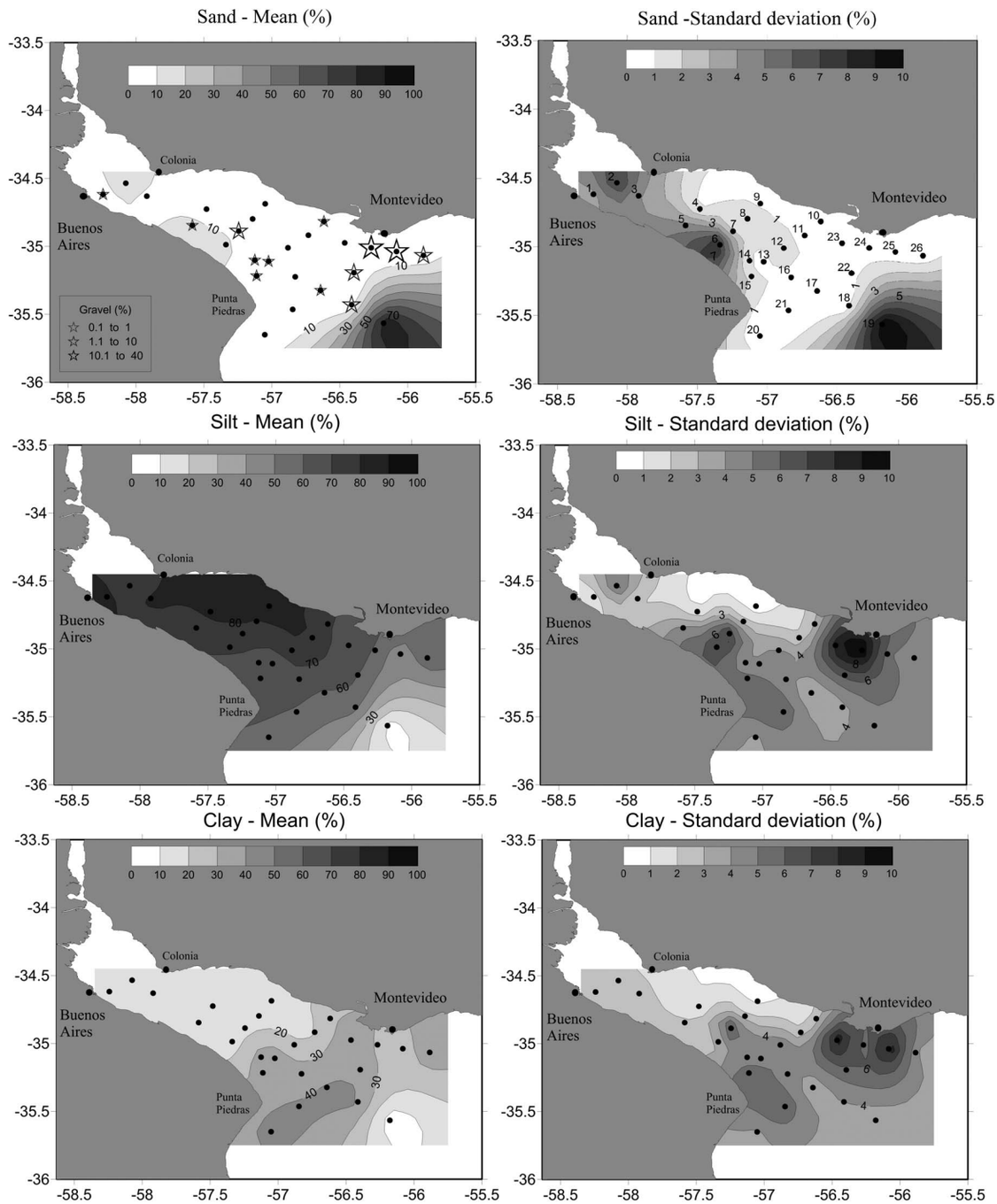

Figure 2. Mean (left panel) and standard deviation between samples (right panel) of the percent concentration of sand (upper panel), silt (middle panel), and clay (lower panel), estimated from the bottom sediment samples gathered during the six cruises of the FREPLATA/FFEM experiment. Stars in the upper left panel represent the mean percentage of gravel.

Stars have been superimposed in the upper left panel of Figure 2 to indicate the regions where very coarse carbonate deposits were found in the samples (bivalve and gastropod shells >2 mm); the size of the stars is proportional to the mean size of those deposits. Values are provided in Table 2. They are more abundant in the northern sector of the exterior estuary, close to Montevideo, with concentrations between 10 and 40%. A much lower percentage is observed to the

Table 2. *Number of sites; percentage of gravel, sand, silt, clay, water, and organic matter content; mean and mode grain size; and standard deviation, degree of sorting, and kurtosis of each bottom sediment sample shown as dots in Figure 1.*

Site	% Gravel	% Sand	% Silt	% Clay	% Water Content	% Organic Matter	Mean Grain Size (μm)	Mode Grain Size (μm)	Standard Deviation σ	Degree of Sorting	Skewness S_k
1	0.62	2.35	83.75	13.29	32.63	1.63	22.67	26.60	15.10	0.67	7.61
2	0.01	21.61	70.72	10.07	31.33	1.43	38.10	53.00	24.69	0.65	6.35
3	0.03	6.63	82.05	11.20	34.74	2.17	29.65	37.60	19.29	0.65	6.96
4	0.00	0.72	84.08	15.17	39.36	2.10	21.66	26.60	14.90	0.69	8.28
5	0.33	14.51	71.89	13.27	35.12	2.18	32.58	53.00	26.32	0.81	9.53
6	0.00	15.56	71.73	12.71	37.81	2.16	34.55	53.00	26.65	0.77	9.63
7	1.23	1.42	78.19	19.16	45.66	3.35	20.65	26.60	16.45	0.80	9.87
8	0.07	7.95	78.84	13.15	38.73	2.44	28.32	26.60	21.52	0.76	10.66
9	0.00	1.04	85.94	13.02	38.94	2.67	24.00	26.60	15.36	0.64	7.71
10	0.89	0.49	70.13	28.50	54.42	4.08	13.52	18.80	11.58	0.86	11.58
11	0.00	0.41	81.06	18.53	44.22	2.77	20.36	26.60	14.73	0.72	8.60
12	0.00	2.15	77.17	20.52	46.27	3.27	22.24	26.60	17.78	0.80	10.07
13	0.19	0.28	61.01	38.51	57.83	4.60	7.62	6.65	6.11	0.80	11.04
14	0.99	0.80	66.31	31.90	59.88	3.64	12.25	13.30	12.69	1.04	16.81
15	0.84	0.00	63.45	35.71	57.29	3.93	9.06	13.30	7.89	0.87	12.48
16	0.00	0.44	65.97	33.60	54.94	4.45	11.51	13.30	11.25	0.98	13.26
17	0.55	0.14	58.14	41.17	60.18	5.91	8.42	6.65	8.46	1.01	15.74
18	2.26	0.00	55.87	41.87	62.47	6.70	6.82	6.65	5.57	0.82	11.70
19	1.04	90.48	4.38	2.69	18.87	0.49	182.40	213.50	85.04	0.47	3.93
20	0.00	0.00	56.83	43.17	64.09	5.40	6.51	6.65	5.10	0.78	11.43
21	0.00	0.00	59.08	40.93	63.02	5.41	7.60	6.65	6.17	0.81	11.30
22	1.56	0.34	61.54	36.57	49.80	4.00	10.87	6.65	11.02	1.01	14.00
23	0.04	0.48	62.63	36.86	53.76	4.44	11.78	6.65	12.20	1.04	13.87
24	10.41	0.41	61.34	27.85	52.43	4.31	11.95	13.30	11.63	0.97	13.92
25	34.29	0.10	40.73	24.88	45.11	5.00	9.66	6.65	9.29	0.96	14.25
26	2.86	0.00	59.93	37.55	53.83	4.17	7.70	6.65	6.17	0.80	11.20

northwest of Punta Piedras, where concentrations are less than 1%.

The mean percent concentration of silt is shown in the central left panel of Figure 2, which shows that this grain texture is present throughout the RDP and constitutes the most abundant sediment in the upper and intermediate estuary. In those regions, a sharp south–north gradient is observed, with an extended maximum over the Ortiz Bank, where concentrations exceed 80%. Here, the standard deviation (Figure 2, central right panel) is very low, indicating low variability between samples. The orientation of the isolines dramatically change seaward of the Barra del Indio shoal, where they align perpendicular to the estuary axis. Here, the concentration rapidly decays offshore. Maximum variability among samples is observed close to Montevideo and to the north of Punta Piedras, even though values are small (<10%).

Finally, the lower left and right panels of Figure 2 show the mean percent concentration and the standard deviation between samples for clay. In this case, a seaward-pointing gradient is observed. The mean concentration of clay maximizes downstream of the Barra del Indio shoal, in the area of the bottom salinity front (see figure 6 of Moreira *et al*., 2013), with values greater than 40%. The standard deviation is less than 7% and maximizes along the imaginary line between Punta Piedras and Montevideo, with absolute maxima close to these locations.

Figure 3 shows the mean percent concentration and standard deviation between samples of the water content (Figures 3a and b) and organic matter content (Figures 3c and d). Numerical values at every station are provided in Table 2. Both distributions resemble those of the clay, suggesting that they could reflect to some extent the effective porosity, in turn related to the degree of compaction, of bottom sediments. Given that the size of the clay is very small, it is more difficult for this type of sediment to compact and expel water; the water content therefore maximizes (>60%; Table 2) where the concentration of that texture is the greatest. The maximum water content variability between samples is observed in the northern exterior estuary close to Montevideo (Figure 3b) in the area related to the wind-forced displacement of the RDP freshwater plume.

Both the concentration of organic matter in the bottom sediment samples and the standard deviation between samples (Figures 3c and d) maximize in a broad area seaward of the Barra del Indio shoal. This region coincides with the area where the water content is largest, where the bottom salinity front is located, and where turbidity rapidly decays toward the sea (see figure 6 of Moreira *et al*., 2013). The maximum mean percentage is 5%, whereas the standard deviation can reach 2.5% (Table 2).

Bottom Sediment Diameter and Degree of Sorting

The mean, mode, standard deviation, and degree of sorting of bottom sediment sizes are given in Table 2 and shown in Figures 4a–d, respectively. To present one and not several similar maps for every cruise, Figure 4 was built after applying an arithmetic mean to the five CILAS distributions available at each of the 26 stations and normalizing the distributions obtained so that the total is 100%. The decision to calculate those averages was taken after having observed, as was shown in the previous section, that the difference between bottom samples in both concentration and grain size distribution is very small. This way, the results of this study must be

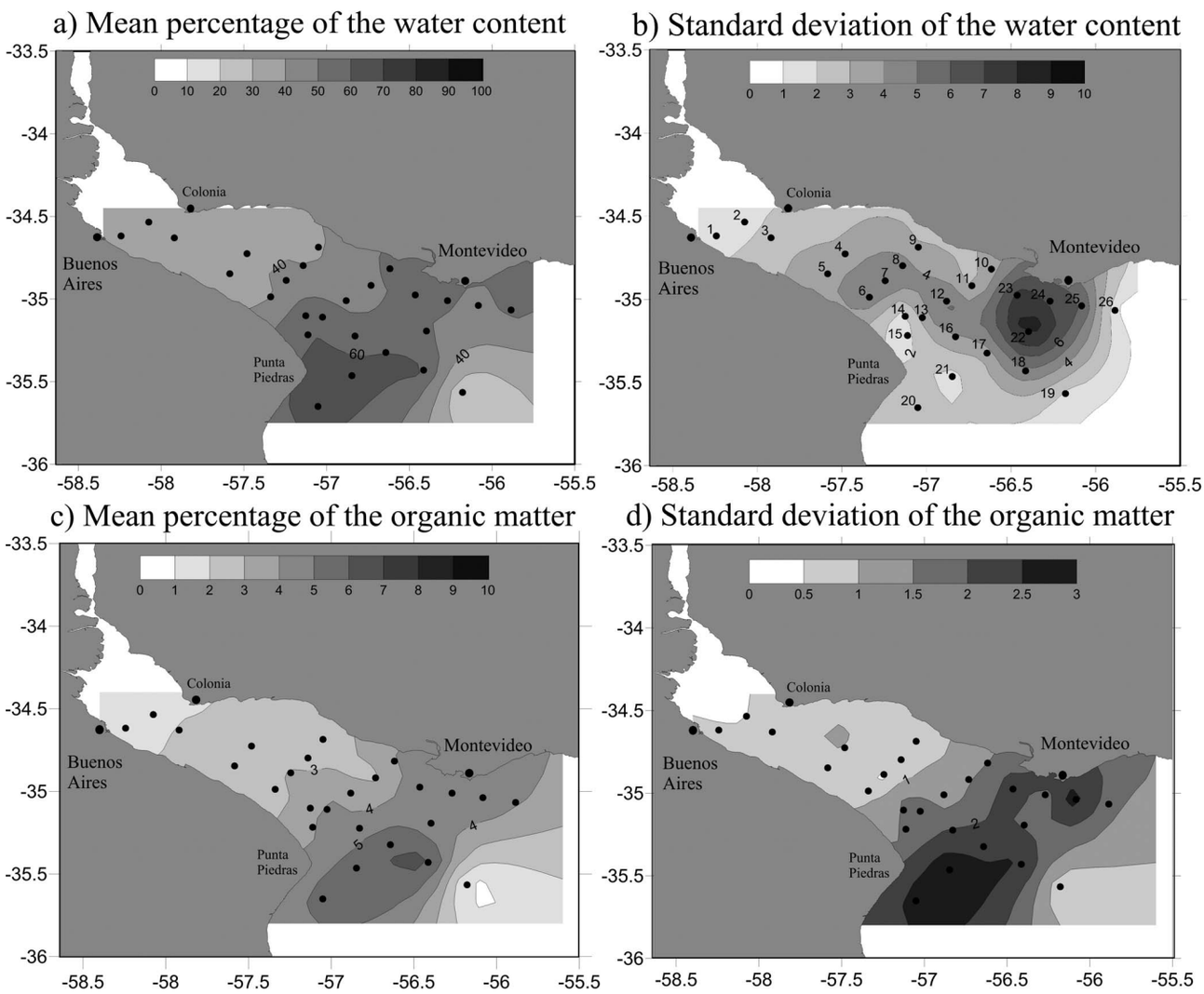

Figure 3. Mean percentage and standard deviation between samples of the water content (a, b) and organic matter (c, d), computed from the bottom sediment samples gathered during the six cruises of the FREPLATA/FFEM experiment.

understood as representing the mean condition over a long period.

Figures 4a and b reveal that the mean and the mode present a similar pattern, with a minimum (<10 μm) seaward of the Barra del Indio shoal, between Punta Piedras and Montevideo. Fine silt and clay with diameters less than 15 μm are present in the bottom sediments in this region, and standard deviation reaches a minimum, with values less than 15 μm. The sediment size increases both upstream and downstream of the Barra del Indio shoal. Coarser sediments (sand with $d_{50} \sim 180$ μm) dominate at the exterior part of the RDP. Upstream of the Barra del Indio shoal, sediment size not only increases, but a small northeast–southwest gradient is observed as well, with a secondary maximum along the Argentinean coast of the intermediate RDP. The mean diameter there is around 40 μm, which corresponds to coarse silt. The standard deviation (Figure 4c) shows a distribution that resembles that of the mode, so that maximum values (15 μm) are observed where the grain size is the largest.

The degree of sorting (Figure 4d) shows a marked gradient in the direction of the estuary axis, with maximum values (corresponding to poorly sorted sediment) offshore of the Barra del Indio shoal and decreasing values upstream and downstream from that area. The absolute minimum (0.5) occurs in the maritime zone, where well-sorted sand is present (Figure 2). Sorting values decrease from the Barra del Indio region toward the inner estuary, indicating that sediments are better sorted there, with more similar sediment sizes. In general, sediments are more poorly sorted

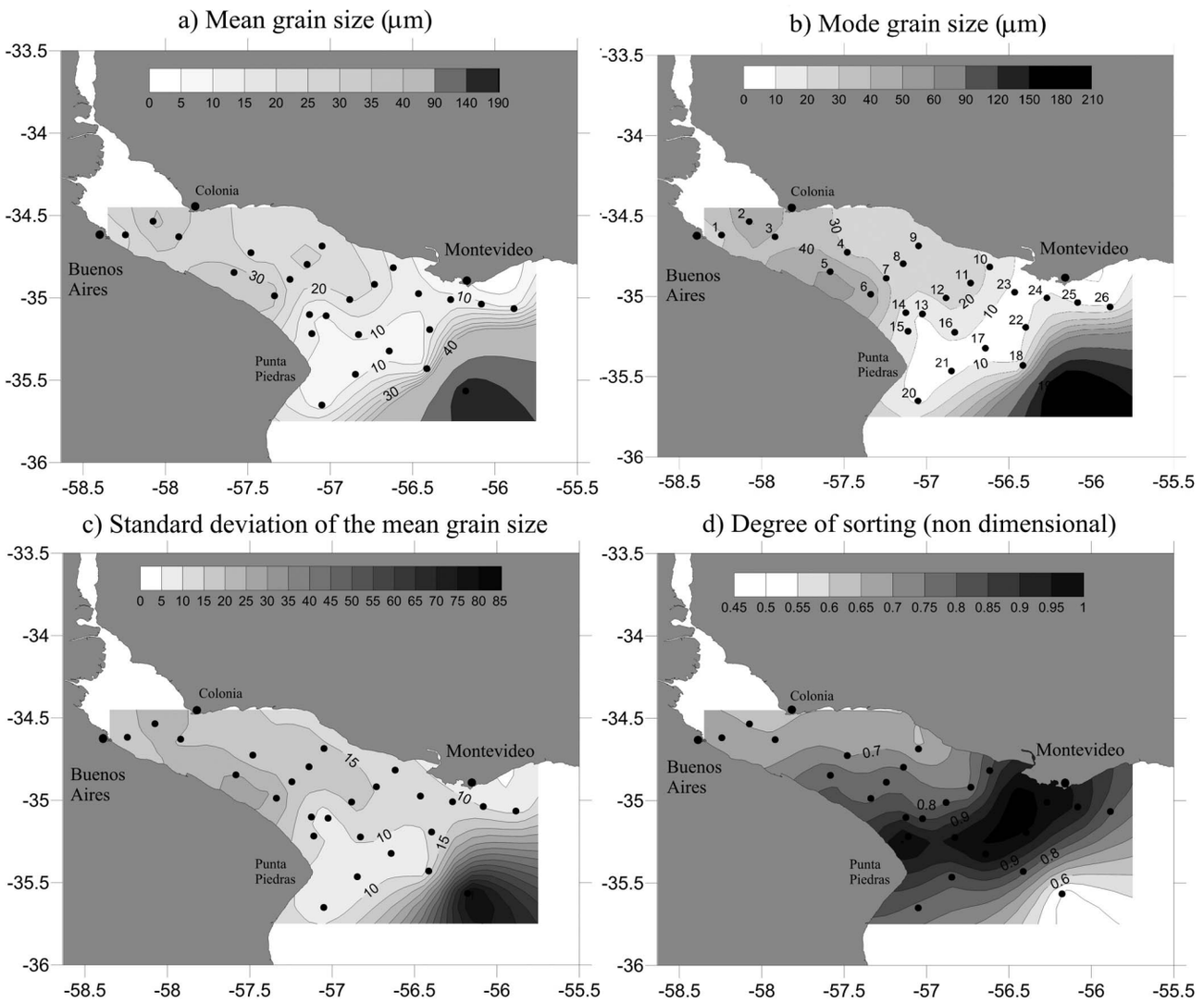

Figure 4. Mean (a) and mode (b) grain size, standard deviation (c), and degree of sorting (d) of bottom sediment size, computed from the bottom sediment samples gathered during the six cruises of the FREPLATA/FFEM experiment.

along the Argentinean coast than along the Uruguayan coast.

Sediment Distribution According to Shepard Classification

The right panel of Figure 5 displays the Shepard classification scheme (without considering shell deposits) calculated for the RDP, whereas the left panel shows a schematic distribution map for the different types of bottom sediments over the estuary, according to that classification. The Shepard scheme (Figure 5, right panel) shows that sediments classified as sand are only present in site number 19 (Figure 5, yellow in the left panel), located in the exterior RDP, and does not seem to have the same origin as the sediments observed in the rest of the estuary. Sandy silt is observed in sites 2, 5, and 6 (Figure 5, dark brown in the left panel), corresponding to the Argentinean coast of the upper and intermediate estuary. Sediments classified as silt are observed in the northern intermediate estuary, over and downstream from the Ortiz Bank in sites 1 (close to Buenos Aires harbor), 3, 4, 7–9, 11, and 12 (Figure 5, dark green in the left panel). Sediments classified as clayey silt are present over and seaward of the Barra del Indio shoal in sites 10, 13–18, 20–23, and 26 (Figure 5, light green in the left panel).

Principal Components Analysis of the Bottom Sediment Distribution

PCA was applied to the $5 \times 26 = 130$ histograms obtained in the CILAS grain size analysis of the samples collected during cruises 2–6 at each of the 26 stations. The aim of this analysis

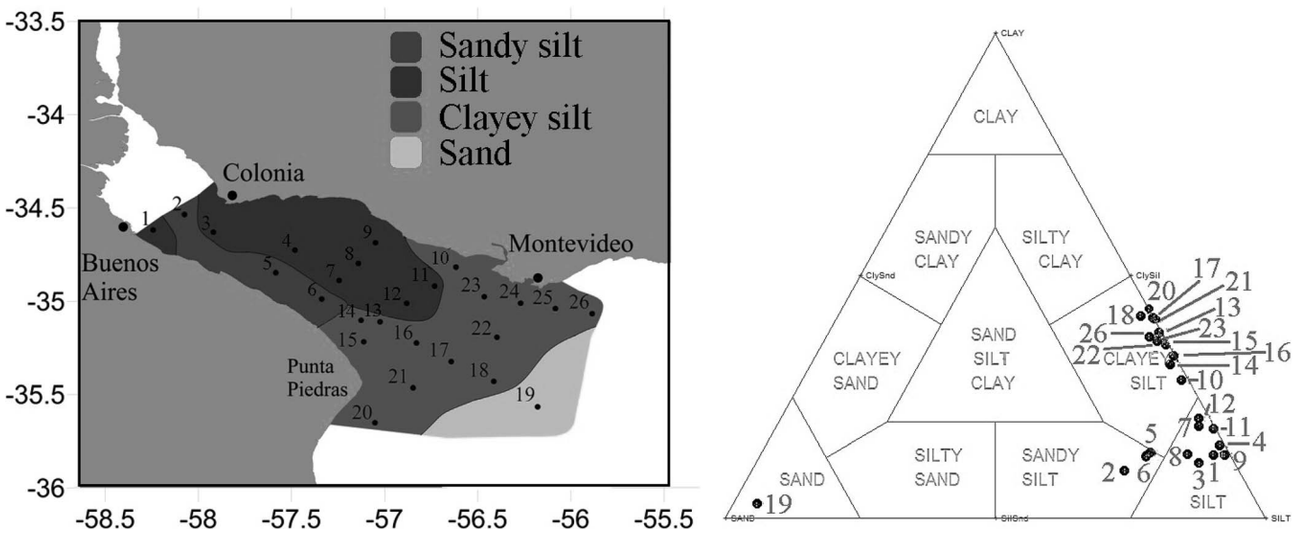

Figure 5. Schematic distribution of the characteristic bottom sediments (left) according to the Shepard (1954) classification scheme (right), computed from the bottom sediment samples gathered during the six cruises of the FREPLATA/FFEM experiment. (Color for this figure is available in the online version of this paper.)

was to reduce the dimensionality of the problem and to investigate whether spatial patterns of homogeneity and significant relationships between stations could be derived, taking into account the small variability between samples observed at each site (see Figure 1). Results are given in Tables 3–5, whereas Figure 6 shows the factor loadings corresponding to each of the three dominant modes. These loadings show areas where the correlation/anticorrelation between the characteristic histogram suggested by the PCs and the real histograms is high. Typically, values are considered significant when the absolute value of the loading exceeds 0.7. To provide an integrated picture, results have been summarized in Figure 7, which schematically displays the five different regions of the estuary identified by the PCA method together with the characteristic of the associated bottom sediments.

Table 3. *Factor loading 1 (varimax normalized) of the principal components of each site and each cruise, with loading ≥ ±0.7 in bold.*

Site	Cruise 2	Cruise 3	Cruise 4	Cruise 5	Cruise 6
1	**−0.96479**	**−0.9775**	**−0.97083**	—	0.26143
2	−0.38421	−0.42378	−0.30048	—	−0.41836
3	−0.65808	**−0.73153**	**−0.83315**	—	**−0.72267**
4	**−0.96781**	**−0.97995**	**−0.97747**	**−0.97966**	**−0.958**
5	−0.20842	−0.45261	**−0.74565**	−0.5667	−0.48362
6	−0.60579	−0.27571	−0.64007	−0.63176	−0.32698
7	0.5386	**−0.94307**	**−0.91794**	**−0.95641**	**−0.94724**
8	**−0.86179**	**−0.85492**	**−0.87058**	**−0.80379**	**−0.84562**
9	**−0.95744**	**−0.98321**	**−0.97722**	**−0.95727**	**−0.96914**
10	0.56913	0.02425	−0.12155	−0.48287	−0.52806
11	**−0.9671**	**−0.97268**	**−0.97731**	**−0.93338**	**−0.97678**
12	**−0.9301**	**−0.95747**	**−0.84219**	−0.6895	**−0.86829**
13	**0.83671**	**0.90223**	**0.85325**	**0.90329**	0.69324
14	**0.84937**	**0.70718**	**0.83119**	**0.83052**	0.40721
15	0.00099	0.40092	**0.77711**	**0.84562**	0.44426
16	**0.86002**	−0.66803	**0.86476**	0.33252	**0.78043**
17	**0.89372**	**0.91479**	**0.71181**	**0.91743**	**0.81071**
18	**0.91892**	**0.90904**	**0.91163**	**0.88839**	**0.8644**
19	0.05914	0.04723	0.05451	0.07894	0.26143
20	**0.92659**	**0.92282**	**0.90541**	**0.91302**	**0.86345**
21	**0.75745**	**0.86115**	**0.91644**	**0.91087**	**0.7679**
22	**0.77904**	**0.80897**	0.55789	0.36785	**0.82549**
23	**0.92633**	**−0.93087**	0.41842	**0.70935**	**0.72816**
24	**0.78142**	0.4987	**0.78924**	−0.03978	−0.10492
25	**0.89361**	**0.92207**	−0.05722	**0.86011**	0.56148
26	**0.91349**	**0.90256**	**0.83035**	**0.73254**	**0.79101**

Table 4. *Factor loading 2 (varimax normalized) of the principal components of each site and each cruise, with loading ≥ ±0.7 in bold.*

Site	Cruise 2	Cruise 3	Cruise 4	Cruise 5	Cruise 6
1	−0.18585	−0.11465	−0.16852	—	−0.44127
2	**−0.84166**	**−0.83214**	**−0.89478**	—	**−0.84995**
3	**−0.71864**	−0.65076	−0.5258	—	−0.65999
4	−0.18032	0.06798	0.12835	−0.02538	−0.24004
5	**−0.78416**	**−0.71516**	−0.54027	**−0.71175**	**−0.75222**
6	**−0.74515**	**−0.84733**	−0.68315	−0.68033	**−0.77891**
7	**0.71924**	−0.26927	−0.34615	0.10614	−0.26216
8	−0.4681	−0.40108	−0.40731	−0.56133	−0.4716
9	−0.23824	−0.10343	−0.15142	−0.24869	−0.19885
10	0.69525	**0.96426**	**0.91928**	**0.83056**	**0.80169**
11	0.13716	−0.0059	−0.12772	0.23478	−0.09328
12	−0.3175	−0.22152	0.32053	−0.4506	−0.42218
13	0.52435	0.31984	0.49425	0.36046	0.69553
14	0.45535	0.66491	0.5186	0.52714	**0.8651**
15	**0.91253**	**0.86559**	0.51494	0.08005	**0.85721**
16	0.43089	0.59619	0.37586	**0.84106**	0.56245
17	0.38709	0.27456	0.48377	0.25928	0.5679
18	0.27355	0.32288	0.2315	0.3733	0.4635
19	−0.17903	−0.16519	−0.13949	−0.15568	−0.44127
20	0.18781	0.2001	0.3443	0.3203	0.4507
21	0.63867	0.45497	0.2841	0.32815	0.6065
22	0.42342	0.13599	0.53375	**0.80368**	0.54033
23	0.17479	0.06237	**0.73066**	0.5837	0.64482
24	0.60186	**0.76506**	0.55352	**0.81012**	**0.95241**
25	0.3661	0.22711	**0.95797**	0.35507	**0.7825**
26	0.32891	0.3059	0.5275	0.65713	0.57013

The first PC (or factor 1; Figure 6a) accounts for 70% of the total variance of the histograms. Grain size distributions of sites 1, 3, 4, 7–9, 11, and 12 (Figure 7, dark green area) are negatively correlated with this PC (Figure 6a, blue), with the highest negative loading of –0.98 observed in the sample collected at site 9 during the third cruise (Table 3). This last station is located to the north of the intermediate estuary, close to the Uruguayan coast and half way between Colonia and Montevideo. Grain size distributions of stations 13–18, 20–23, and 26 (Figure 7, light green area) are positively correlated with factor 1 (Figure 6a, red). The highest correlation between the mode and the histograms is observed for site 20 (located to the southeast of Punta Piedras), with a maximum of +0.93 for the sample gathered during the second cruise (Table 3).

The second PC (or factor 2; Figure 6b) accounts for 20% of the total variance of the set of histograms. This mode correlates

Table 5. *Factor loading 3 (varimax normalized) of the principal components of each site and each cruise, with loading ≥ ±0.7 in bold.*

Site	Cruise 2	Cruise 3	Cruise 4	Cruise 5	Cruise 6
1	0.157907	0.156525	0.148459	—	**−0.719189**
2	0.083755	0.099508	0.073235	—	0.102905
3	0.143127	0.144615	0.143014	—	0.146126
4	0.156943	0.17619	0.156294	0.175489	0.148918
5	0.021854	0.01635	0.159329	0.100998	0.1092
6	0.135331	0.019676	0.162253	0.164789	−0.063008
7	0.186467	0.162584	0.172742	0.234076	0.168412
8	0.128725	0.176415	0.090682	0.119257	0.100997
9	0.138609	0.134937	0.134805	0.137886	0.137774
10	0.272432	0.178061	0.202144	0.175765	0.173224
11	0.183173	0.193572	0.152722	0.231648	0.155777
12	0.161281	0.16285	0.352532	0.233449	0.190869
13	0.109596	0.065039	0.1038	0.103469	0.130165
14	0.119707	0.143978	0.088715	0.126353	0.191601
15	0.231021	0.143393	0.14954	0.175012	0.143326
16	0.213003	0.219793	0.110308	0.215236	0.159173
17	0.091802	0.064204	0.095498	0.103519	0.108964
18	0.085248	0.093242	0.056273	0.092054	0.113338
19	**−0.938256**	**−0.957957**	**−0.902948**	**−0.967963**	**−0.719189**
20	0.075201	0.068723	0.077695	0.078792	0.117211
21	0.121898	0.092799	0.07527	0.084221	0.13556
22	0.127436	0.079924	0.150879	0.266417	0.116368
23	0.070288	0.191964	0.122911	0.2163	0.172065
24	0.129257	0.232898	0.189693	0.407132	0.1663
25	0.084436	0.098192	0.17802	0.10268	0.183794
26	0.086579	0.087666	0.118786	0.132872	0.13974

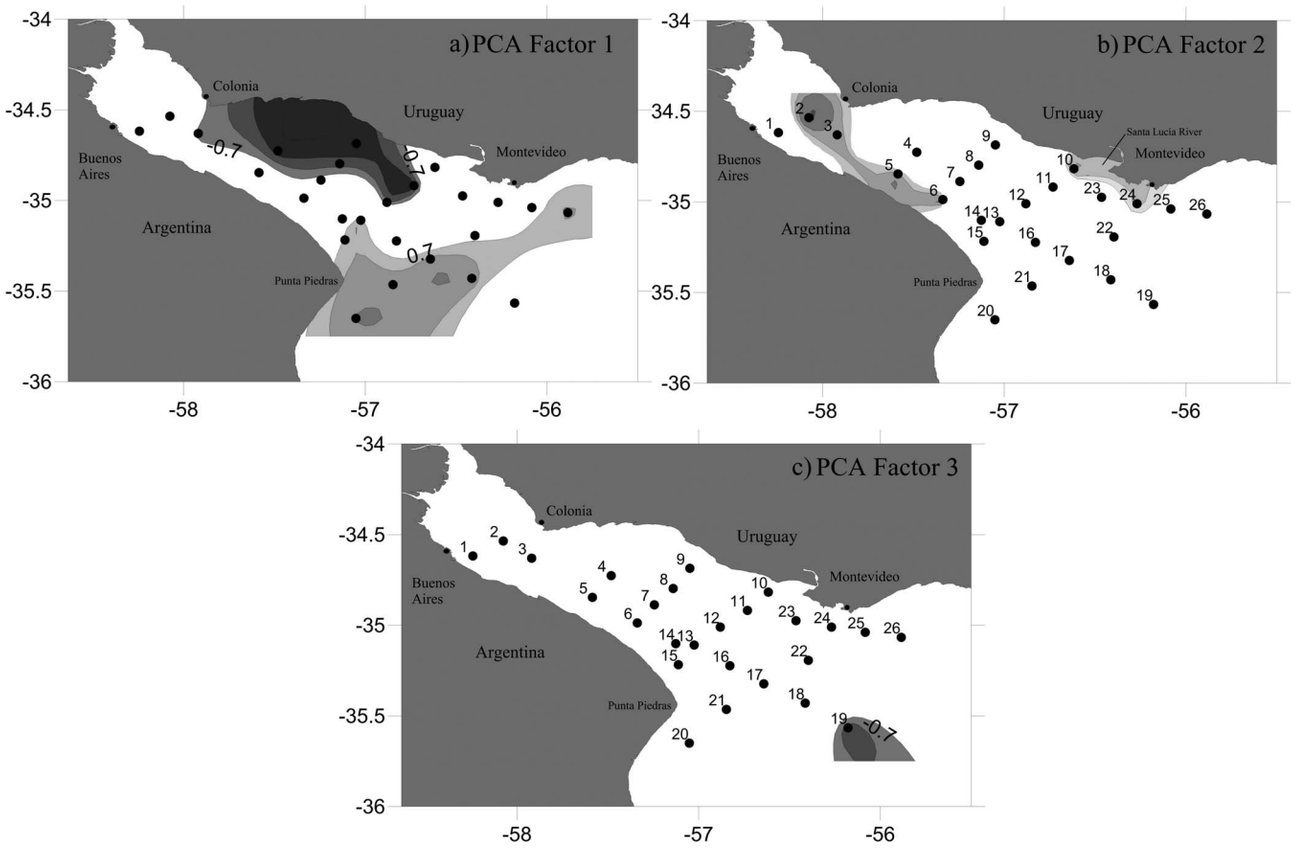

Figure 6. Factor loadings of the PCA analysis. Upper left PCA factor 1, upper right PCA factor 2, and lower panel PCA factor 3. Values are considered significant when the absolute value of the loading exceeds 0.7. Red color represents the positive loading and blue represents the negative phase. (Color for this figure is available in the online version of this paper.)

positively (Figure 6b, red) with the observations gathered at stations 10, 24, 25, and, partly, 23 (Figure 7, orange area). The highest positive loading occurs for site 10, with a maximum of +0.96 for the sample collected during the third cruise (Table 4). Those four sites are located along the northern coast of the intermediate RDP between the Santa Lucía River mouth and Montevideo. Factor 2 is negatively correlated (Figure 6b, blue) to grain size distributions of sites 2, 5, and 6 (Figure 7, dark brown area); the highest loading is observed for site 2 with a value of –0.89 during the fourth cruise (Table 4). Those sites are located along the southern coast of the upper intermediate estuary.

Finally, the third PC (or factor 3; Figure 6c) accounts for 5% of the total variance. This mode is negatively correlated with the grain size distribution of site 19 (Figure 6c, blue), with a value of –0.97 for the sample collected during the fifth cruise (Table 5). This point is located at the exterior RDP (Figure 7, yellow area).

In this way, the PCA analysis reduced the 130 samples to five characteristic histograms describing the typical bottom sediment distributions of the RDP. To show real histograms and not the PCA modes (which can be difficult to interpret in physical terms), Figure 8 shows the characteristic grain size distributions for the five regions identified from the PCA and represented by the histogram most highly correlated with the modes, according to Tables 3–5.

The positive phase of factor 1 (Figure 8a), represented by site 20 cruise 2, corresponds to a region where sediments are typically clayey silt (mixed sediment, ~54% silt and ~46% clay, very poorly sorted) with very fine silts and clays (<5 μm). Hereinafter, this area is referred to as "Barra del Indio region" (Figure 7, light green area).

The negative phase of factor 1 is represented by site 9 cruise 3 (Figure 8b). It is a zone where sediments are typically silt (similar size sediment, <1% sand, ~85% silt, and ~14% clay, well sorted) with medium and fine silts of diameters 10–30 μm. In what follows, this region is referred to as the "northern coast of the intermediate RDP" (Figure 7, dark green area).

The positive phase of factor 2 is represented by site 10 cruise 3 (Figure 8c), where typical sediments are clayey silt (more mixed sediment, <1% gravel, ~68% silt, and ~31% clay, poorly sorted). The grain size distribution indicates that the sediments are medium and fine silt (diameters up to 30 μm) with a percentage of clay (diameters of 0.1–0.4 μm). This zone has

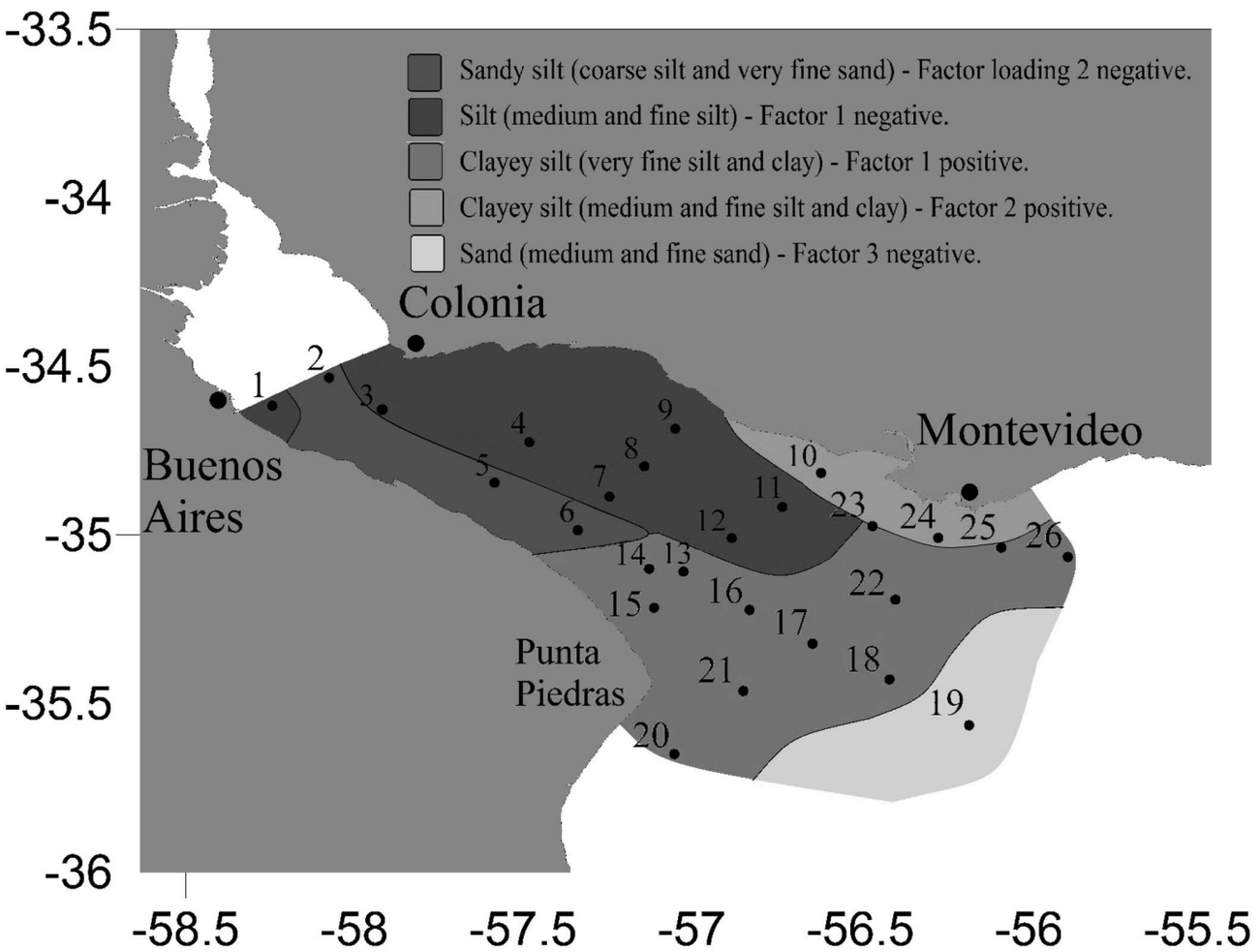

Figure 7. Schematic distribution of the areas where data correlates well with the different factors derived from the PCA analyses applied to the grain size histograms derived from the CILAS analysis of the bottom sediment samples gathered during the six cruises of the FREPLATA/FFEM experiment. (Color for this figure is available in the online version of this paper.)

more silt than the area associated with the positive phase of factor 1 (Figure 8b). This area is referred to as the "Santa Lucía region" (Figure 7, orange area).

The negative phase of factor 2 (Figure 8d), represented by site 2 cruise 4, is characterized by sandy silt (mixed sediments, ~19% sand, ~72% silt, and ~9% clay, poorly sorted). This area is referred to as the "southern coast of the intermediate RDP" (Figure 7, dark brown area). Grain size distribution for this region shows mean diameters of 30–60 μm for the coarse silts and up to 80 μm for the very fine sands; sediments here are coarser than in the previously mentioned areas.

Finally, the negative phase of factor 3 (Figure 8e), represented by site 19 cruise 5, is characterized by sand (~94% sand, ~3% silt, and ~3% clay, well sorted) with medium and fine sands. The mean grain diameter for this region is about 200 μm, the largest in the observations of this study. This area is referred to as the "exterior RDP" (Figure 7, yellow region).

Suspended Sediment Distribution for the Identified Main Zones of the Río de la Plata

To complement the study of the bottom sediment grain size distribution and favor the understanding of the underlying processes, characteristic grain size distributions of the suspended sediments derived from water samples collected at the same stations as bed samples are also analyzed. Even though some differences were observed between suspended sediment samples at each location between cruises (especially in what regards the sediment concentrations; see Moreira *et al.*, 2013), the general conclusions extracted from the analysis below, regarding granulometry, do not change significantly. Therefore, the histograms belonging to the sites and cruises that maximize the correlation with every phase of the PC modes in the former section are shown and discussed. Results (Figure 9) show that over the five areas characterized in the previous section, the grain size distri-

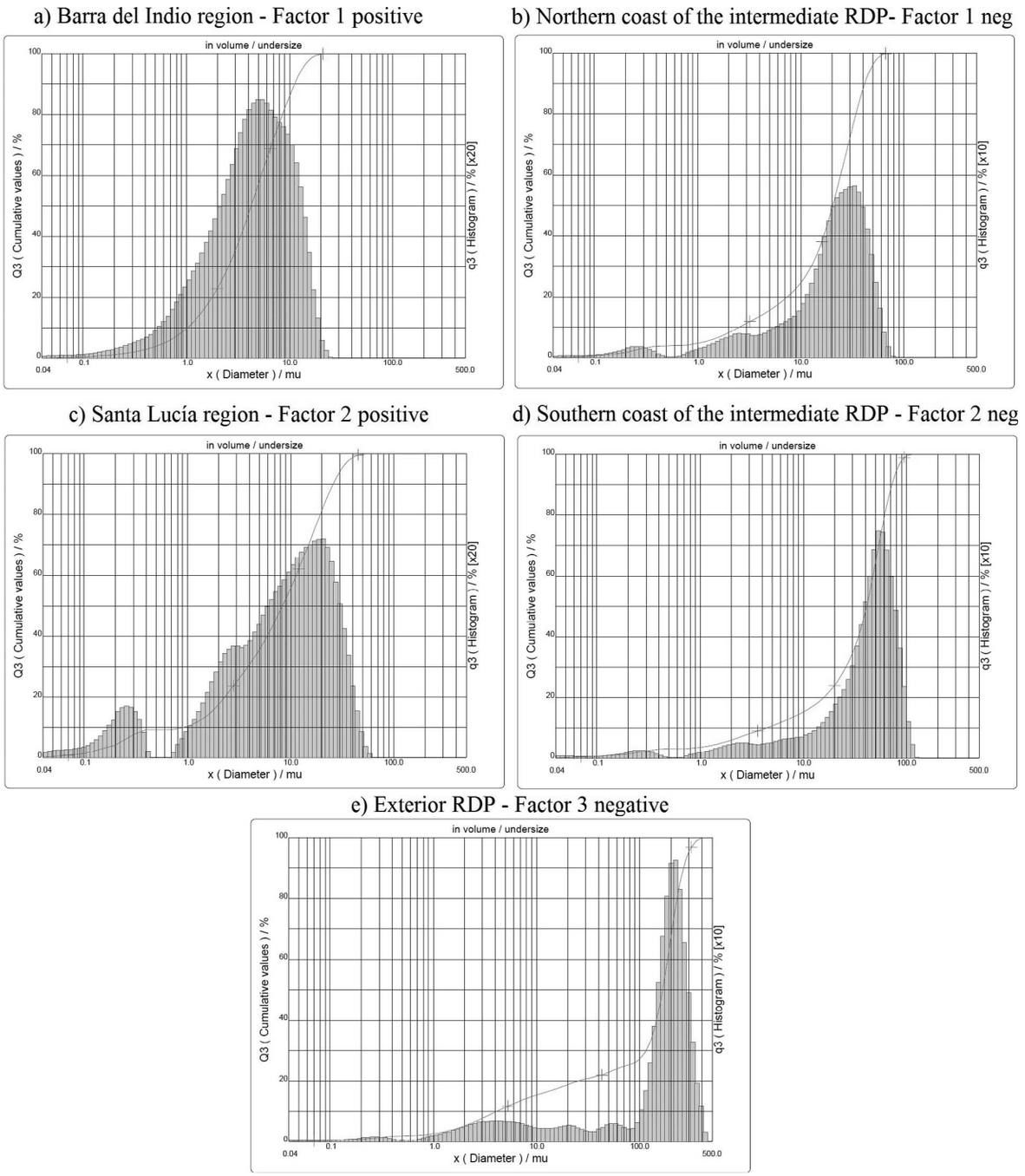

Figure 8. Grain size distribution of the bottom sediment samples for (a) factor 1 positive, site 20, cruise 2, Barra del Indio region (light green in Figure 7); (b) factor 1 negative, site 9, cruise 4, northern coast of the intermediate RDP (dark green in Figure 7); (c) factor 2 positive, site 10, cruise 4, Santa Lucía region (orange in Figure 7); (d) factor 2 negative, site 2, cruise 4, southern coast of the intermediate RDP (dark brown in Figure 7); and (e) factor 3 negative, site 19, cruise 4, exterior RDP (yellow in Figure 7).

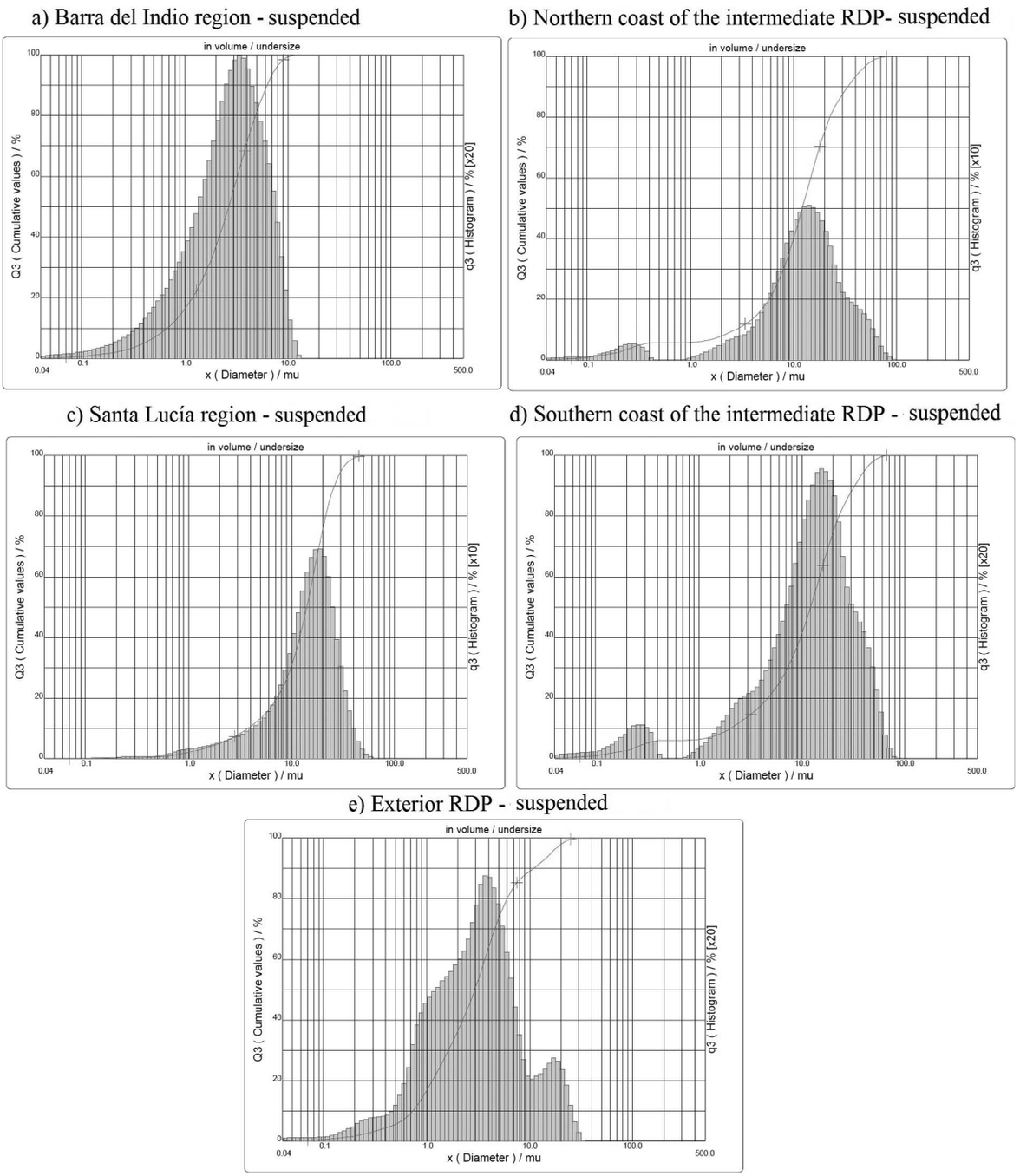

Figure 9. Grain size distribution of the suspended sediment samples for (a) Barra del Indio region (light green in Figure 7), site 20, cruise 2; (b) northern coast of the intermediate RDP (dark green in Figure 7), site 9, cruise 4; (c) Santa Lucía region (orange in Figure 7), site 10, cruise 4; (d) southern coast of the intermediate RDP (brown in Figure 7), site 2, cruise 4; and (e) exterior RDP (yellow in Figure 7), site 19, cruise 4.

bution of the suspended sediments present thinner particles than the bottom sediment; the histograms displayed by Figure 9 correspond to the same sites and cruises as those of Figure 8. The following can be observed:

Over the Barra del Indio region (Figure 9a) suspended sediments correspond to ~30% silt and ~70% clay, or silty clay in the Shepard classification. Compared with the bottom sediments (Figure 8a), there is less silt and more clay in

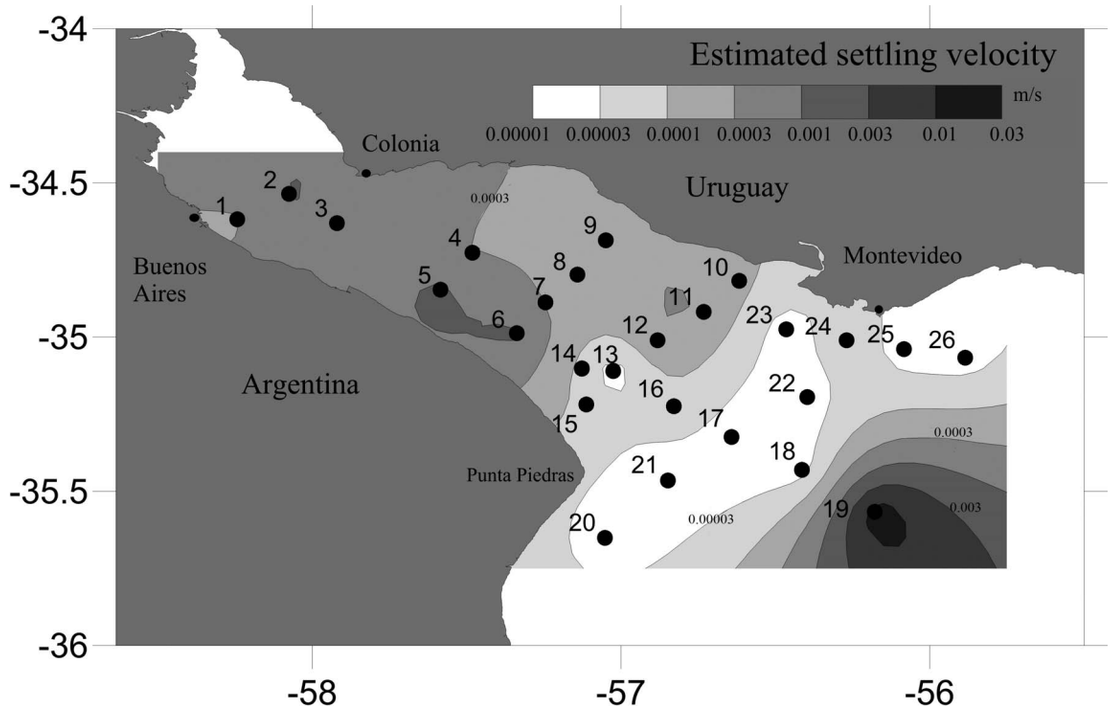

Figure 10. Estimated settling velocity of the suspended sediments (ms^{-1}).

suspension in the suspended sediments. This is consistent with the nature of the sediments: the thinner particles remain in suspension, whereas the coarser ones settle to the bottom.

In the northern coast of the intermediate RDP region (Figure 9b), the Shepard classification of the suspended sediments is silt (~1% sand, ~86% silts, and ~13% clays), similar to the bottom sediment classification (Figure 8b). The grain size distributions differ in the presence of finer silts, with diameters between 5 and 15 μm in the suspended sediments.

The Santa Lucía area (Figure 9c) is characterized silt-type suspended sediments according to the Shepard classification, whereas the bottom sediments were classified as clayey silts. This is because there is more silt and less clay in the suspended sediments (~87% silt and ~13% clay). The grain size histograms of the suspended and bottom sediments samples are, therefore, different. The diameter of the suspended particles goes up to 20 μm, with a lower percentage of coarse clay (~1 μm) than in the bottom sediments.

For the southern coast of the intermediate RDP region (Figure 9d), the Shepard classification identifies silt, whereas the bottom sediments are sandy silt. The grain size distribution of the suspended sediments shows less sand ($\ll$1%) and more silt and clay (~82% and ~17%, respectively). Figure 9d shows that the mean diameter of the suspended sediments (ranging from 5 to 20 μm) is thinner than for the bottom sediments, with a larger percentage of fine sediment (clays with diameters ~0.3 μm).

Finally, in the exterior RDP region (Figure 9e), the analysis reveals a completely different grain size distribution between the suspended and bottom sediments. Here suspended sediments have a very low percentage of sand (<1%) and abundant silt and clay (~67% and ~32%, respectively). They correspond to clayey silt in the Shepard classification, which is very different from the sandy sediments identified in the bottom samples. Bottom sediments (diameters between 100 and 200 μm) are much coarser than the suspended sediments (diameters from 0.8 to 20 μm), which must have a different origin and have been, obviously, advected there.

To complement the analysis, Figure 10 shows the settling velocity of the suspended sediments computed from their dominant textures (Figure 4, mode). To favor interpretation, the color scale is logarithmic. The highest settling velocities are observed at the exterior estuary (station 19), where relatively coarse sands abound. The lowest velocities occur, in contrast, seaward of the Barra del Indio, in the region of the salt wedge, where the dominant texture is clay. Toward the intermediate and upper estuary, the settling velocities increase, even though a gradient in the direction perpendicular to the estuary axis seems to be present. Nonetheless, when analyzing this figure, it must be taken into account that it was built using only the characteristics of the dominant sediments and without taking into account the estuary's dynamics.

Net Sediment Transport Pathways

The data set of computed grain size parameters was used in a trend analysis to determine statistically possible net sediment transport pathways. To define the trend and transport vectors, the characteristic distance D_{CR} of 60 km has been chosen,

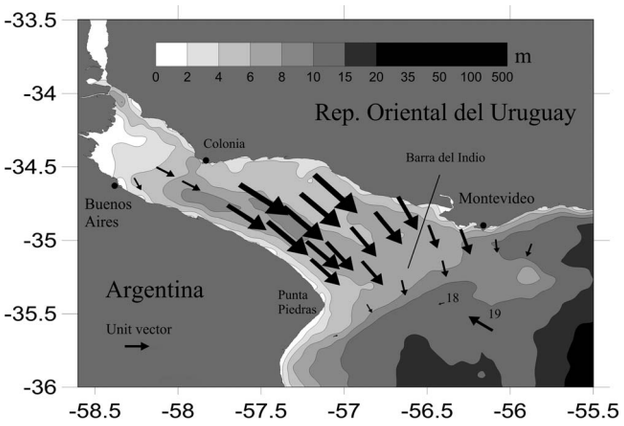

Figure 11. Distribution of statistical net transport vectors and bathymetry in the Río de la Plata estuary.

which is slightly larger than the maximum sampling interval for this particular investigation (~45 km). Therefore, any two samples with a distance less than 60 km were compared. Transport vectors were derived according to Equations (6) and (7). The identified residual grain size trends (Figure 11) show a highly ordered pattern, with a characteristic (nondimensional) vector length (L) of 1.35, estimated according to Equation (8).

The statistical net sediment transport patterns, represented by the grain size trends, reveal several distinctive characteristics. First, in most of the RDP, the sediment transport seems to be toward the southeast (*i.e.* seaward). This is the case for every sampled point, with the exception of station 19, for which the model suggests upstream transport. A slight upstream transport is obtained for station 18, but the associated vector length is very small, almost negligible. Figure 11 also reveals that the statistical net sediment transport increases from the estuary head to the intermediate RDP, and then it decreases again up to the Barra del Indio shoal. This suggests a convergence in this last area.

The transport divergence suggested by Figure 11 between stations 1, 2, and 3 and those located immediately downstream seems to be a mathematical artifact rather than a real feature, because only a few measurements were taken in the upper estuary.

DISCUSSION

This section synthesizes the results with theoretical arguments to provide an integrated view of the hypothesized processes and determines the bottom sediment distribution in the RDP.

The trend vector analysis (Figure 11) suggests that along the upper and intermediate estuary, up to the Barra del Indio shoal, sediments are transported to the southeast. Sediment distributions (Figure 2) show that bottom sediments have a gradational arrangement of textures, from silt and sandy silt in the intermediate estuary, to clayey silt and clay in the area of the bottom salinity front. Along the estuary, sediments become progressively less sorted (Figure 4d), and the water and organic matter content increase (Figures 3a and c), both maximizing in the area of the salt wedge. In agreement, the estimated settling velocities reduce (Figure 10). Seaward of the salt wedge, well-sorted coarser sand dominates (Figure 2a), and the content of water and organic matter decays again (Figures 4a and c). The characteristics of the sediments in this area differ from those found in the suspended sediments in the entire estuary (Figure 9). Here, the trend vector analysis suggests a reversion in the transport (Figure 11) and, therefore, convergence. Along the northern coast of the estuary, between the Santa Lucía River mouth and Montevideo (Figure 7), suspended sediments are thinner than the bottom sediments (Figures 8c and 9c). Coarse deposits (carbonate shell) are more abundant in the northern sector of the exterior estuary, seaward of Montevideo, whereas a much lower percentage is observed to the northwest of Punta Piedras.

The results of the PCA (Figures 7–9) and theoretical arguments, some of them already suggested in previous works and others set up here for the first time, drive to the conclusion that, as regards bottom sediments, the RDP can be divided into at least five different regions where sedimentological processes seem to be strongly influenced by the hydrodynamics.

The Paraná River Delta Front/Playa Honda

Previous studies have shown that the fine sands carried by the RDP main tributaries are deposited at the estuary head (not sampled during the FREPLATA/FFEM experiment), forming the Paraná River Delta and Playa Honda (Brea, Busquets, and Spalletti, 1999). The fine sands remain in suspension within the tributary rivers because of the high levels of turbulence they encounter (Brea, Busquets, and Spalletti, 1999), but they quickly settle to the bottom when the width and the depth of the estuary increase, which leads to a decrease in the currents speed (Moreira *et al.*, 2013; Simionato *et al.*, 2004; Simionato, Meccia, and Dragani, 2009). Coarser sands, transported as bed load, also settle in that region with deposits that have been estimated to reach 15 million ton y^{-1} (Amsler, 1995; Amsler and Drago, 1988). This mechanism permits a rapid seaward growth of the Paraná River Delta. At the present growing rate, the Delta could reach the city of Buenos Aires by the end of this century (Sarubbi, 2007). Most of the sand, therefore, is deposited within the Delta and its front, which explains why the sediments transport beyond, to the areas studied in this work, include a relatively small percentage of sand, but mainly silt and clay.

The Intermediate RDP

This section in turn can be split into northern and southern parts. Here, silt—with percentages greater than 70%—predominates over clay and sand (Figure 2). The concentration of clay becomes progressively larger seaward, so that in the area of the bottom salinity front (immediately offshore of the Barra del Indio shoal), bottom sediments comprise almost equal parts fine silt and clay (Figures 7 and 8). The progressive dominance in the intermediate estuary of those much finer sediments might be explained by clay, smaller and lighter than the silt, remaining in suspension for a longer time and traveling farther away from the source (Figure 10); Additionally, the mean current speed in the RDP rapidly decays offshore as the estuary becomes broader and depth increases (Simionato *et al.*, 2004;

Simionato, Meccia, and Dragani, 2009), favoring deposition. However, the analysis shows a marked gradient in the characteristics of bottom sediment mixtures between the northern and southern portions of the intermediate RDP (Figures 2, 5, and 6) that cannot be explained only in terms of a generalized reduction of mean transport offshore. The northern coast of the intermediate estuary is characterized by well-sorted sediments, including more than 85% silts, with sizes between 10 and 30 μm (Figures 2, 4, 7, and 8b). The southern coast, instead, is characterized by coarser and less well sorted sediments, with diameters between 30 and 60 μm (Figures 2, 4, 7, and 8d). In this last region, even though more than 70% of the bottom sediments are silt, the percentage of sand reaches almost 20%. This distribution of sediments cannot be accounted for in terms of the settling velocities of the suspended sediments (Figure 10). The dominant suspended sediments are coarser along the southern coast of the estuary than along the northern coast (Figures 9b and d); therefore, settling velocities increase, in average, toward the south (Figure 10). Here, then, the estuarine dynamics must play a significant role. In this sense, two processes can be identified which, acting either individually or synergistically, might account for the following differences observed.

Differences in the Pathways of the Freshwater Plumes of the Main Tributaries through the Estuary

This mechanism was suggested by Parker *et al*. (1987). The Uruguay and Paraná Guazú (the mightiest branch of the Paraná) river waters flow along the northern estuary, whereas the waters of the other branch of the Paraná (Paraná de las Palmas) follow the southern coast (Simionato, Meccia, and Dragani, 2009). Right before its convergence with the RDP estuary, the Paraná de las Palmas receives the waters of the Luján River. This is a minor tributary with a much lower runoff, but which drains waters and sediments from the Pampas and whose influence is obvious in other properties of the southern portion of the RDP, such as the low conductivity (Simionato, Meccia, and Dragani, 2009). Moreira *et al*. (2013), additionally suggested this as one of the possible reasons why the concentration of suspended sediments is larger along the southern than along the northern coast of the estuary yearlong.

Differences in Tidal Hydrodynamics

Tidal currents are much stronger along the southern coast of the RDP than along the northern coast (Simionato *et al*., 2004). Moreira *et al*. (2013) suggested that this could be an additional cause for the higher concentrations of suspended sediments observed along the Argentinean coast compared with the Uruguayan coast. The hypothesis is that the stronger tidal currents along the southern coast of the RDP might also inhibit suspended sediment deposition or cause resuspension; this way, suspended sediments could be transported further downstream. In contrast, along the northern coast over the shallow Ortiz Bank region, tidal currents are weaker and sediments might be able to settle. In this sense, it is worthwhile to mention that Moreira *et al*. (2013) showed that tidal currents are fundamental for resuspending sediments in the water column in the RDP, whereas wind moves them to the surface.

At and Immediately Seaward of the Barra del Indio Shoal

In the region of the bottom salinity front, the percentage of clay in the bottom sediments rises to more than 45% (Figures 2 and 8a), and the water and organic matter content reach their maximum (Figures 3a and c). The suspended sediments are also thinner (Figure 9a), and the settling velocity is the weakest in the RDP (Figure 10). The presence of finer and cohesive bottom sediments in this area might be due, at least in part, to the salinity increase (Moreira *et al*. 2013) and the associated physicochemical flocculation processes, which are supposed to become important in this region, leading to deposition of the clay (Ayup, 1986, 1987; Parker *et al*., 1987). The estuary depth and width also increase markedly in this region, leading to a very significant reduction of currents (Simionato *et al*., 2004) and favoring deposition. Being finer, the sediments of this region are more porous, and therefore water content is higher (Figure 3a). This region is also characterized by an increase in the number of living organisms, as revealed by the organic matter concentration in the bottom sediments (Figure 3c), which is consistent with an increase in light penetration related to the reduction of the suspended sediment concentration and, therefore, of turbidity (Framiñan *et al*., 1996; Moreira *et al*., 2013) and the availability of nutrients transported from the continent. The RDP estuary presents two sources of organic matter: phytoplankton and plant detritus (Acha *et al*., 2008). In the Barra del Indio region, a high density of the copepod *Acartia tonsa*—up to 8,000 ind m^{-3}—and mysid *Neomysis americana*—up to 2,520 ind m^{-3}—has been observed (Mianzan *et al*., 2001; Schiariti *et al*., 2006). They are omnivorous and could take advantage of the abundance of organic matter in the detritic form (Acha *et al*., 2008).

Area between the Santa Lucía River Mouth and Montevideo

Our analyses also reveal the presence of a different bottom sediment texture along the northern coast of the estuary, in the area between the Santa Lucía River mouth and Montevideo (Figures 7 and 8c). Here the bottom sediments are poorly mixed and composed of fine silt (~70%) and clay (the remaining 30%). The particular composition of those sediments, which do not shown coherence with the suspended sediment characteristics in this area (Figure 9c), suggests that bottom sediments are relict. Parker *et al*. (1987) suggested the occurrence of a region with relict muds along the northern coast of the RDP, even though they locate it offshore and upstream of the Santa Lucía River mouth.

Exterior Estuary to the Southeast of the Bottom Salinity Front

Finally, the results show that in the exterior estuary, to the southeast of the bottom salinity front, coarse sands with grain sizes between 170 and 200 μm dominate (Figures 2, 7, and 8e). This sands are much coarser than those transported by the RDP (Figure 9e), indicating that they must come from the adjacent shelf. In fact, these sands with $d_{50} \sim 180$ μm are characteristic of the maritime zone (Parker *et al*., 1987; Ottman and Urien, 1966). The absence of typical RDP sediments in this region (Figure 8) also suggests that the offshore limit of the significant RDP sediment deposits, forming the submerged

delta, occurs just upstream in association with the salt wedge and the flocculation region. This hypothesis is supported by the net transport vector analysis (Figure 11), which indicates in that area a reversion of transport and, therefore, convergence.

CONCLUSIONS

In this paper, a new data set of bottom sediment properties derived from samples collected in the upper and intermediate Río de la Plata estuary during an international project are analyzed. The aims are to provide a comprehensive and objective characterization of the bottom sediment long-term mean distribution, to study their composition, and to continue the construction of a conceptual model of the involved physical mechanisms. This data set provided, for the first time, simultaneous observations of the granulometric distribution of the bottom and suspended sediments and of water and organic matter content in the bottom sediments, which advances the understanding of the diverse processes that determine the observed mean distribution. Moreover, the new samples were analyzed utilizing the CILAS technique, which allowed the application of more robust statistical methods (*e.g.*, PCA) to characterize areas with similar bottom sediment distributions objectively. Finally, the homogeneity of sampling permitted the construction of the first net sediment transport vector diagram for the region.

Results show that the bottom sediments have a gradational arrangement of textures as they are transported seaward, from dominant sand at the head, silt in the intermediate estuary and clayey silt and clay at its mouth. Textures become progressively poorly sorted offshore, and the water and organic matter content increases; consistently, the settling velocity decays. The distributions of water and organic matter content resemble those of the clay, suggesting that they could reflect to some extent the degree of compaction of bottom sediments. Coarse deposits (carbonate shell) are more abundant in the northern sector of the exterior estuary, close to Montevideo, and a lower percentage is observed to the northwest of Punta Piedras.

The distribution patterns inferred for the textures seem to be strongly related to the geometry and what is known about the hydrodynamics in the estuary. Along the northern coast of the intermediate RDP, well-sorted medium and fine silt predominates, whereas along the southern coast, coarser and less sorted silt prevails. This could be due to differences in tidal currents or the riverine water pathways, or both, along the coasts, depending on their source. Around the Barra del Indio shoal, clay prevails over silt and sand, and the water and organic matter content reaches a maximum. Physicochemical flocculation processes probably become important there, and the width and the depth of the estuary also largely increase, producing a significant reduction in the currents. Immediately seaward of the salt wedge, net transport reverses its direction, and well-sorted, coarser sand dominates. This sand is much coarser than the sediment transported by the RDP tributaries, suggesting that it comes from the adjacent shelf. Between the Santa Lucía River mouth and Montevideo, a different type of sediment is observed, consisting of poorly sorted fine silt and clay, that seems to be relict sediment. The inferred net transport suggests convergence immediately offshore of the Barra del Indio shoal, which is consistent with the constant growing of the banks observed in the Río de la Plata.

The results discussed above not only complement but also validate some of the hypothesis set up by Parker *et al.* (1987) in their pioneer study. Their figure 3 (provided as Supplementary Material), which schematically shows their conclusions regarding the genetic association of the sediments based on the limited information available for those times, has many aspects in common with Figure 7 of this study, based on an objective study of a homogeneous set of samples analyzed with modern methods. In this sense, this study supports most of the Parker *et al.* conclusions and provides further evidence about other possible mechanisms influencing bottom sediment textures in the RDP.

Even though Moreira *et al.* (2013) found a strong seasonal cycle in the concentration of suspended sediments in the RDP, this study did not find any clear seasonal cycle in the bottom sediments; moreover, as shown in Figures 1 and 2, variability between samples is low. Even though there are reasons to believe that the deposition of sediments in the RDP could vary through the year, the identification of such processes would demand a very specific sampling over a long period of time, which was out of the scope and possibilities of this experiment. Nevertheless, it can be regarded as an important issue in future studies.

During the revision process, the question arose about the possibility of human actions interfering with the parameters, specifically in the PCA. The proximity of some points to Montevideo and Buenos Aires could be important to this explanation. Even though the possibility cannot be tested with the samples collected and the analysis made here, it should be further explored in the future.

This paper not only contributes to a better understanding of the sedimentological processes in this important estuary, but it will help in the construction and validation of numerical models, which are needed for management and scientific purposes. Those studies, including future sediments and biogeochemical modeling, are envisaged as a continuation of this research. They will be, in turn, the necessary first step toward estimation of the land-to-ocean fluxes in this important system.

ACKNOWLEDGMENTS

This study was funded by the FFEM (Fonds Français pour l'Environnement Mondial of France) in the framework of the PNUD/GEF RLA/99/G31 FREPLATA project, the ANPCyT (National Agency for Scientific and Technological Research of Argentina) PICT 2010-1831 and PICT 2014-2672 projects, and the CONICET (National Council for Scientific and Technological Research of Argentina) PIP 112 201101 00176 projects. Diego Moreira's and Moira Luz Clara Tejedor's participation were also allowed by Universidad de Buenos Aires and CONICET Ph.D. fellowships, respectively.

LITERATURE CITED

Acha, M.E. and Macchi, G.J., 2000. Spawning of Brazilian menhaden, *Brevoortia aurea*, in the Río de la Plata estuary off Argentina and Uruguay. *Fishery Bulletin*, 98(2), 227–235.

Acha, M.E.; Mianzan, H.; Guerrero, R.; Carreto, J.; Giberto, D.; Montoya, N., and Carignan, M., 2008. An overview of physical and ecological processes in the Rio de la Plata Estuary. *Continental Shelf Research*, 28(13), 1579–1588.

Amsler, M., 1995. *Carga de Lavado del Río Paraná en Sus Tramos Medio e Inferior, Origen, Comportamiento Anual,Cconcentraciones y Caudales Sólidos. Análisis del Avance del Frente del Delta del Río Paraná*. Ezeiza, Argentina: Laboratorio de Hidráulica del Instituto Nacional del Agua (INA), *Technical Report*, 48p.

Amsler, M. and Drago, E., 1988. Suspended sediment at a cross section of the middle Paraná River: Concentration, granulometry and influence of the main tributaries. *In:* Bordas, M.P. and Walling, D.E. (eds.), *Sediment Budgets: Porto Alegre Symposium, Brazil*, *1988: IAHS Publication No. 174*. Porto Alegre, Brazil: International Association of Hydrological Sciences, pp. 381–396.

Ayup, R.N., 1986. Comportamento dos sedimentos emsuspensao no Río de la Plata exterior e proximidades. *Pesquisas Sección B Ciências Naturais* (Porto Alegre, Brazil), 18, 39–68.

Ayup, R.N., 1987. Intercambio sedimentar entre o Río de la Plata Exterior e a plataforma continental adjacente. *Pesquisas Sección B Ciências Naturais* (Porto Alegre, Brazil), 19, 106–206.

Balay, M.A., 1961. *El Río de la Plata Entre la Atmósfera y el Mar. Publicación H-621*. Buenos Aires, Argentina: Servicio de Hidrografía Naval, Armada Argentina, *Technical Report*, 153p.

Berasategui, A.D.; Acha E.M., and Fernandez Araoz, N.C., 2004. Spatial patterns of ichthyoplankton assemblages in the Río de la Plata estuary (Argentina-Uruguay). *Estuarine Coastal and Shelf Science*, 60(4), 599–610.

Berasategui, A.D.; Menu Marque, S.; Gómez-Erache, M.; Ramírez, F.C.; Mianzan, H.W., and Acha, E.M., 2006. Copepod assemblages in a highly complex hydrographic region. *Estuarine Coastal and Shelf Science*, 66(3), 483–492.

Brea, J.; Busquets, M., and Spalletti, P., 1999. *Generación y Transporte de Sedimentos en la Alta Cuenca del Río Bermejo. Impacto en la Hidrovía, Delta del Paraná y Río de la Plata*. Programa Estratégico de Acción para la Cuenca del Río Bermejo, Capítulo C. Comisión Binacional para el Desarrollo de la Alta Cuenca del Río Bermejo y el Río Grande de Tarija, pp. 221–238.

Campos, J.D.; Lentini, C.A.; Miller, J.L., and Piola, R.A., 1999. Interannual variability of the sea surface temperature in the South Brazilian Bight. *Geophysical Research Letters,* 26(14), 2061–2064.

Canevari, P.; Blanco, D.; Bucher, E.; Castro, G., and Davidson, I., 1998. *Los Humedales de la Argentina. Clasificación, Situación Actual, Conservación y Legislación*. Buenos Aires, Argentina: Wetlands Internacional and Secretaría de Recursos Naturales y Desarrollo Sustentable de la Nación, *Publication 46*, 208p.

Cardini, J.C.; Garea, M., and Campos, M.R., 2002. Modelación del transporte de sedimentos puestos en suspensión por actividades de dragado en el Río de la Plata, para la generación en tiempo real de pronósticos de afectación de áreas costeras. *Proceedings of the Congreso de Mecánica Computacional* (Santa Fé- Paraná, Argentina), 21, pp. 2325–2342.

CARP (Comisión Administradora del Río de la Plata), 1989. *Estudio para la Evaluación de la Contaminación en el Río de la Plata*. Montevideo, República Oriental del Uruguay: Comisión Administradora del Río de la Plata.

Cheng, P.; Gaob, S., and Bokuniewicz, H., 2004. Net sediment transport patterns over the Bohai Strait based on grain size trend analysis. *Estuarine, Coastal and Shelf Science*, 60(2), 203–212.

Codignotto, J.O.; Dragani, W.C.; Martin, P.B.; Simionato, C.G.; Medina, R.A., and Alonso, G., 2012. Wind wave climate change and increasing erosion observed in the Río de la Plata, Argentina. *Continental Shelf Research*, 38, 110–116. doi:10.1016/j.csr.2012.03.013

Colombo, J.C.; Cappelletti, N.; Barreda, A.; Migoya, M.C., and Skorupka, C., 2005. Vertical fluxes and accumulation of PCBs in coastal sediments of the Río de la Plata estuary, Argentina. *Chemosphere*, 61(9), 1345–1357.

Colombo, J.C.; Cappelletti, N.; Migoya, M.C., and Speranza, E., 2007. Bioaccumulation of anthropogenic contaminants by detritivorous fish in the Río de la Plata estuary: 2-Polychlorinated biphenyls. *Chemosphere*, 69(8), 1253–1260.

Depetris, P.J. and Griffin, J.J., 1968. Suspended load in the Río de la Plata drainage basin. *Sedimentology*, 11(1–2), 53–60.

Fossati, M.; Cayocca, F., and Piedra-Cueva, I., 2014. Fine sediment dynamics in the Río de la Plata. *Advances in Geosciences*, 39, 75–80.

Framiñan, M.B. and Brown, O.B., 1996. Study of the Río de la Plata turbidity front: I. Spatial and temporal distribution. *Continental Shelf Research*, 16(10), 1259–1282.

Framiñan, M.B.; Etala, M.P.; Acha, M.E.; Guerrero, R.A.; Lasta, C.A., and Brown, O.B., 1999. Physical characteristics and processes of the Río de la Plata estuary. *In:* Perillo, G.M.; Piccolo, M.C., and Pino Quivira, M. (eds.), *Estuaries of South America: Their Morphology and Dynamics*. New York: Springer, pp. 161–194.

Framiñan, M.B.; Valle-Levinson, A.; Sepúlveda, H.H., and Brown, O.B., 2008. Tidal variations of flow convergence, shear, and stratification at the Rio de la Plata estuary turbidity front. *Journal of Geophysical Research: Oceans*, 113(8). doi:10.1029/2006JC004038

Gao, S. and Collins, M., 1991. A critique of the "McLaren Method" for defining sediment transport paths. *Journal of Sedimentary Petrology*, 61(1), 143–146.

Gao, S. and Collins, M., 1992. Net sediment transport patterns inferred from grain-size trends, based upon definition of "transport vectors." *Sedimentary Geology*, 80(1–2), 47–60.

Glorioso, P.D. and Flather, R.A., 1995. A barotropic model of the currents off SE South America. *Journal of Geophysical Research*, 100(C7), 13427–13440.

Glorioso, P.D. and Flather, R.A., 1997. The Patagonian Shelf tides. *Progress in Oceanography*, 40(1), 263–283.

Gómez-Erache, M., 1999. Spatial and temporal variation in the copepod community of Montevideo Bay, Uruguay. *Proceedings of the Seventh International Conference on Copepoda* (Curitiba, Brazil), pp. 25–31.

Gómez-Erache, M.; Sans, K.; Danilo, C., and Menu Marque, S., 2004. Recent data on freshwater cyclopoid copepods (Cyclopoida: Cyclopidae) from Uruguay. *Nauplius*, 11(2), 145–148.

Guerrero, R.A.; Acha, E.M.; Framiñan, M.B., and Lasta, C.A., 1997. Physical oceanography of the Río de la Plata estuary, Argentina. *Continental Shelf Research*, 17(7), 727–742.

Huret, M.; Dadou, I.; Dumas, F.; Lazure, P., and Garçona, V., 2005. Coupling physical and biogeochemical processes in the Río de la Plata plume. *Continental Shelf Research*, 25(5–6), 629–653.

Jaime, P.R. and Menéndez, A.N., 2002. *Análisis del Régimen Hidrológico de los ríos Paraná y Uruguay*. Ezeiza, Argentina: Instituto Nacional del Agua (INA), *Technical Report LHA-01-216-02,* 42p.

Jaureguizar, A.; Bava, J.; Carozza, C., and Lasta, C., 2003a. Distribution of the whitemouth croaker (*Micropogonias furnieri*) in relation to environmental factors at the Río de la Plata Estuary, South America. *Marine Ecololgy Progress Series*, 255, 271–282.

Jaureguizar, A.; Menni, R.; Bremec, C.; Mianzan, H., and Lasta, C., 2003b. Fish assemblage and environmental patterns in the Río de la Plata estuary. *Estuarine, Coastal and Shelf Science*, 56(5–6), 921–933.

Jaureguizar, A.; Militelli, M., and Guerrero, R., 2008. Distribution of *Micopogonias furnieri* at different maturity stages along an estuarine gradient and in relation to environmental factors. *Journal of the Marine Biological Association*, 88(1), 175–181.

Lasta, C., 1995. La Bahía Samborombón: Zona de Desove y Cría de Peces. La Plata, Argentina: Universidad Nacional de La Plata, Ph.D. dissertation, 304p.

López Laborde, J., 1987a. Distribución de sedimentos superficiales de fondo del Río de la Plata Exterior y Plataforma adyacente. *Investigaciones Oceanológicas*, 1(1), 19–30.

López Laborde, J., 1987b. Caracterización de los sedimentos superficiales de fondo del Rio de la Plata exterior y plataforma adyacente. *Anales Científicos Universidad Nacional Agraria La Molina*, 11, 33–47.

López Laborde, J. and Nagy, G.J., 1999. Hydrography and sediment transport characteristics of the Río de la Plata: A review. *In:* Perillo, G.M.E.; Piccolo, M.C., and Pino, M. (eds.), *Estuaries of*

South America: Their Geomorphology and Dynamics. New York: Springer, pp. 133–160.
McLaren, P., 1981. An interpretation of trends in grain-size measurements. *Journal of Sedimentary Petrology*, 51, 611–624.
McLaren, P. and Bowles, D., 1985. The effects of sediment transport on grain-size distributions. *Journal of Sedimentary Petrology*, 55, 457–470.
McManus, J., 1988. Grain size determination and interpretation. *In:* Tucker, M. (ed.), *Techniques in Sedimentology*. Oxford: Blackwell, pp. 63–85.
Meccia, V.L.; Simionato, C.G.; Fiore, M.M.E.; D'Onofrio, E., and Dragani, W.C., 2009. Sea surface height variability in the Río de la Plata estuary from synoptic to inter-annual scales: Results of numerical simulations. *Estuarine, Coastal and Shelf Science*, 85(2), 327–343.
Meccia, V.L.; Simionato, C.G., and Guerrero, R., 2013. The Río de la Plata estuary response to wind variability in synoptic time scale: Salinity fields and breakdown and reconstruction of the salt wedge structure. *Journal of Coastal Research*, 29(1), 61–77. doi:10.2112/JCOASTRES-D-11-00063.1
Menéndez, A.; Re, M.; Sarubbi, A., and García, P., 2009. A conceptual model for sediment transport in the inner Plata River. *Proceedings of the 6th Symposium on River, Coastal and Estuarine Morphodynamics*, RCEM (Santa Fe, Argentina, International Association on Hydraulic Engineering and Research), p. 23.
Menéndez, A.N. and Sarubbi, A., 2007. A model to predict the Paraná Delta Front advancement. *Workshop on Morphodynamic Processes in Large Lowland Rivers* (Santa Fe, Argentina), p. 25.
Mianzan, H.W.; Lasta, C.; Acha, E.M.; Guerrero, R.; Machi, G., and Bremec, C., 2001. The Río de la Plata estuary, Argentina, Uruguay. *In:* Seeliger, U.; de Lacerda, LD., and Kjerve, B. (eds.), *Ecological Studies: Coastal Marine Ecosystems of Latin America*. Berlin: Springer, pp. 185–204.
Moreira, D.; Simionato, C.G.; Gohin, F.; Cayocca, F., and Luz Clara Tejedor, M., 2013. Suspended matters mean distribution and seasonal cycle in the Río de la Plata estuary and the adjacent shelf from MODIS and *in situ* observations. *Continental Shelf Research*, 68, 51–66.
O'Connor, W.P., 1991. A numerical model of tides and storm surges in the Río de la Plata estuary. *Continental Shelf Research,* 11(12), 1491–1508.
Ottman, F. and Urien, C.M., 1965. La melange des eaux douces et marines dans le Río de la Plata. *Cahiers Oceanographiques*, 17(10), 213–234.
Ottman, F. and Urien, C.M., 1966. Sur quelques problemas sedimentologiques dans le Río de la Plata. *Revue de Géographie Physique et Géologie Dynamique*, 8(3), 209–224.
Parker, G.; Cavalloto, J.L.; Marcolini, S., and Violante, R., 1986a. Los registros acústicos en la diferenciación de sedimentos subácueos actuales (Río de la Plata). *Proceedings of the 1er Reunión de Sedimentología* (La Plata, Argentina), pp. 42–44.
Parker, G.; Cavalloto, J.L.; Marcolini, S., and Violante, R., 1986b. Transporte y dispersión de los sedimentos actuales del Río de la Plata (análisis de texturas). *Proceedings of the 1er Reunión de Sedimentología* (La Plata, Argentina), pp. 38–41.
Parker, G. and López Laborde, J., 1989. *Estudio para la Evaluación de la Contaminación en el Río de la Plata, Aspectos Geológicos*. CARP-SHIN-SOHMA, Informe de Avance a la Comisión Administradora del Río de La Plata, *Report*, pp. 1–72.
Parker, G.; Marcolini, J.; Cavalloto, J., and Violante, R., 1987. Modelo esquemático de dispersión de sedimentos en el Río de la Plata. *Ciencia y Tecnología del Agua*, 1(4), 68–80.
Preisendorfer, R.W., 1988. *Principal Component Analysis in Meteorology and Oceanography*. Amsterdam: Elsevier, 425p.
Rodrigues, K.A., 2005. Biología Reproductiva de la Saraquita, Ramnogasterarcuata del Estuario del Río de la Plata. Mar del Plata, Argentina: University of Mar del Plata, Argentina, Master's thesis, 40p.
Sarubbi, A., 2007. Análisis del Avance del Frente del Delta del Río Paraná. Buenos Aires, Argentina: Universidad de Buenos Aires, Facultad de Ingeniería, Degree thesis, 136p.
Schiariti, A.; Berasategui, A.D.; Giberto, D.A.; Guerrero, R.A.; Acha, E.M., and Mianzan, H.W., 2006. Living in the front: *Neomysis americana* (Mysidacea) in the Río de la Plata estuary, Argentina, Uruguay. *Marine Biology*, 149(3), 483–489.
Sepúlveda, H.H.; Valle-Levinson, A., and Framiñan, M.B., 2004. Observations of subtidal and tidal flow in the Río De La Plata estuary. *Continental Shelf Research*, 24(4–5), 509–525.
Shepard, F.P., 1954. Nomenclature based on sand–silt–clay ratios. *Journal of Sedimentary Petrology*, 24, 151–158.
Shiklomanov, I.A., 1998. *A Summary of the Monograph "World Water Resources": A New Appraisal and Assessment for the 21st Century*. Paris: United Nations Educational, Scientific and Cultural Organization, p. 37.
Simionato, C.G.; Dragani, W.C.; Meccia, V.L., and Nuñez, M.N., 2004. A numerical study of the barotropic circulation of the Río de la Plata estuary: sensitivity to bathymetry, Earth rotation and low frequency wind variability. *Estuarine, Coastal and Shelf Science*, 61, 261–273.
Simionato, C.G.; Meccia, V.L., and Dragani, W.C., 2009. On the path of plumes of the Río de la Plata estuary main tributaries and their mixing time scales. *Geoacta*, 34(2), 87–116.
Simionato, C.G.; Meccia, V.L.; Dragani, W.C.; Guerrero, R., and Nuñez, M.N., 2006a. The Río de la Plata estuary response to wind variability in synoptic to intra-seasonal scales: Barotropic response. *Journal of Geophysical Research*, 111(C9), C09031. doi:10.1029/2005JC003297
Simionato, C.G.; Meccia, V.; Dragani, W., and Nuñez, M.N., 2006b. On the use of the NCEP/NCAR surface winds for modeling barotropic circulation in the Río de la Plata estuary. *Estuarine, Coastal and Shelf Science*, 70, 195–206. doi:10.1016/j.ecss.2006.05.047
Simionato, C.G.; Meccia, V.L.; Guerrero, R.A.; Dragani, W.C., and Nuñez, M.N., 2007. The Río de la Plata estuary response to wind variability in synoptic to intra-seasonal scales: 2. Currents' vertical structure and its implications for the salt wedge structure. *Journal of Geophysical Research*, 112(C7), C07005. doi:10.1029/2006JC003815
Simionato, C.G.; Moreira, D.; Piedra Cueva, I.; Fossati, M.; Guerrero, R.; de los Campos, T.; Balestrini, C.; Cayocca, F.; Gohin, F., and Repecaud, M., 2011a. Proyecto FREPLATA—FFEM Modelado Numérico y Mediciones *in-situ* y Remotas de las Transferencias de Sedimentos Finos a través del Río de la Plata. Parte A: Adquisición de Datos. *Frente Marítimo*, 22, 109–136.
Simionato, C.G.; Moreira, D.; Re, M., and Fossati, M., 2011b. *Estudio de la dinámica hidro-sedimentológica del Río de la Plata: Observación y modelación numérica de los sedimentos finos*. Buenos Aires: Proyecto FREPLATA, CTMFM-CARP, 109p.
Simionato, C.G.; Nuñez, M.N., and Engel, M., 2001. The salinity front of the Río de la Plata—A numerical case study for winter and summer conditions. *Geophysical Research Letters*, 28(13), 2641–2644.
Simionato, C.G.; Vera, C.S., and Siegismund, F., 2005. Surface wind variability on seasonal and interannual scales over Río de la Plata area. *Journal of Coastal Research*, 21(4), 770–783.
Simionato, C.G.; Clara Tejedor, M.L.; Campetella, C.; Guerrero, R.; and Moreira, D., 2010. Patterns of sea surface temperature variability on seasonal to sub-annual scales at and offshore the Río de la Plata Estuary. *Continental Shelf Research,* 30(19), 1983–1997.
Skene, D.; Ryan, D.; Brooke, B.; Smith, J., and Radke, L., 2005. The Geomorphology and Sediments of Cockburn Sound. *Geoscience Australia, Record 2005/10*, 90p.
Syvitski, J.P.M., 2003. Supply and flux of sediment along hydrological pathways: Research for the 21st century. *Global and Planetary Change,* 39(1–2), 1–11.
Urien, C.M., 1966. *Distribución de los Sedimentos en el Río de la Plata Superior*. Boletín Servicio de Hidrografía Naval, *Technical Report 3*, pp. 197–203.
Urien, C.M., 1967. *Los Sedimentos Modernos del Río de la Plata Exterior*. Argentina: Servicio de Hidrografía Naval, *Público H-106*, *Technical Report 4*, pp. 113–213.

Urien, C.M., 1972. Río de la Plata estuary environments. *Geological Society of America Memoirs*, 133, 213–234.

USGS CMGP (U.S. Geological Survey Coastal and Marine Geology Program), 2014. *Woods Hole Coastal and Marine Science Center Sediment Grain-Size Analysis Software*. http://woodshole.er.usgs.gov/software/sediment-software.html.

Walling, D.E. and Webb, B.W., 1996. Erosion and sediment yield: A global overview. *In:* Walling, D.E. and Webb, B.W. (eds.), *Global and Regional Perspective*. Exeter, U.K.: IAHS Publication 236, pp. 73–84.

Wentworth, C.K., 1922. A scale of grade and class terms for clastic sediments. *Journal of Geology*, 30(5), 377–392.

Queries for coas-32-06-05

This manuscript/text has been typeset from the submitted material. Please check this proof carefully to make sure there have been no font conversion errors or inadvertent formatting errors. Allen Press.